CIMAT

Centro de Investigación en Matemáticas, A.C.

Discrete Exterior Calculus applications for Transport equation

T E S I S

Que para obtener el grado de

Maestro en Ciencias

con especialidad en

Computación y Matemáticas Industriales

Presenta

Marco Antonio Flores Pérez

Director de Tesis:

Dr. Salvador Botello Rionda

Co-director de Tesis:

Dr. Rafael Herrera Guzmán

Autorización de la versión final

Guanajuato, Guanajuato, octubre de 2022

Agradecimientos

Primero, quiero agradecer a mi familia y a mis amigos por todo su apoyo durante mi experiencia en CIMAT. Especialmente quiero agradecer a mi hermana Karen, mis amigos Zaira Martínez, César García y Laura Pérez ya que han sido un gran soporte para mí durante las altas y bajas de estos dos años.

A la psicóloga Mayté González, quien durante el primer año de la maestría me permitió mantener el nivel requerido en la maestría en sus sesiones, las cuales me dieron herramientas que seguiré utilizando en mi vida personal y profesional.

A mis asesores, el Dr. Salvador Botello y el Dr. Rafael Herrera por el tiempo que me otorgaron, su apoyo y por compartir su conocimiento para el desarrollo de esta tesis.

A CONACyT, por su apoyo económico para que pudiera llevar a cabo mis estudios de maestría.

Contents

List of Figures

Chapter 1

Introduction

Discrete exterior calculus (DEC) is a relatively new numerical method first proposed by Hirani in his PhD thesis in 2003 [1]. It is based on exterior differential calculus, a theory that generalizes differentiation and integration to curved spaces or manifolds, which are of great relevance in physical theories such as gravitation and cosmology. It is not surprising that such a physically important mathematical theory would lead to a discrete theory that allows the development of a numerical method for solving partial differential equations (PDEs).

In his original work, Hirani presented DEC as a purely theoretical model, which can be seen as differential calculus over finite *simplicial complexes*[1] of arbitrary dimension. He also explained that DEC can be applied to variational problems. The first article where DEC was used as a numerical method was published in 2015 where Darcy's law was solved [2] and from then on, DEC has been used successfully for the solutions of several PDE such as Maxwell equations [3], Navier-Stokes equations [4] to mention a few examples.

[1] Triangular mesh built from domain

In this thesis, we focus our attention on solving the Transport equation with dominant advection. This is a continuation of Noguez's work [5], where he proposed a discretization of the Transport equation for arbitrary velocity vector fields. Our main contribution is the application of a correction scheme to the artificial diffusion technique for DEC and the Finite element method (FEM). We use FEM results in order to asses the performance of DEC.

Chapter 2 explains the basic theory of DEC, the Transport equation and some techniques used when dominant advection is considered. Chapter 3.1 describes the DEC-discretization of the Transport equation and presents a comparision with FEM for the discretized advection and diffusion terms. Numerical examples are shown in chapter 4 and conclusions are given in chapter 5.

Chapter 2

Theoretical Framework

In order to describe the transport equation using DEC, we need to explain forst some concepts of Differential Exterior Calculus such as the exterior derivative, the wedge product and the Hodge star operator. Although DEC can be applied in any dimension, for the sake of simplicity, we will explain the aforementioned concepts in 2 dimensions.

2.1 Differential Exterior Calculus

As previously mentioned, Differential Exterior Calculus is a subject in differential geometry. Differentials are defined as linear mappings from tangent spaces to the real numbers. Differential forms are linear functionals whose arguments are $k-$dimentional volumes. For example, let $f : \mathbb{R}^n \to \mathbb{R}$ be a smooth function. We can integrate f along a curve (using a $1-$form) and over a surface (using a $2-$form) by taking the integrals (2.1a) and (2.1b), respectively

$$\int f(\boldsymbol{x}) dl, \tag{2.1a}$$

$$\int f(\boldsymbol{x}) dS, \tag{2.1b}$$

where $\boldsymbol{x} \in \mathbb{R}^n$, dl is a $1-$form and dS is a $2-$form.

One important property of integrals is that they take orientation into account. For instance, consider a line integral along a curve from point A to point B. If we calculate the integral but along the same curve but in the oppsite direction, we will get

$$\int_A^B f(\boldsymbol{x})dl = -\int_B^A f(\boldsymbol{x})dl. \tag{2.2}$$

The same happens with surface integrals. Let $\boldsymbol{u} : \mathbb{R}^2 \to \mathbb{R}^2$ be a smooth vector field, then the integral

$$\iint \boldsymbol{u}(\boldsymbol{x}) \cdot \boldsymbol{n} dS, \qquad \boldsymbol{n} \text{ is the unit normal to the surface,} \tag{2.3}$$

changes sign if we perform the dot product with the reverse direction of the normal vector $-\boldsymbol{n}$. Note that the orientation of the surface is determined by the choice of normal vector.

2.1.1 Differential Forms

Let $\{\boldsymbol{d}x^i\}_{i=1}^n$ be the basic $1-$forms for $\mathbb{R}^n$ and $\boldsymbol{u} \in \mathbb{R}^n$. We have

$$\boldsymbol{d}x^i(\boldsymbol{u}) = u^i, \tag{2.4}$$

where u^i is the $i-$th component of $\boldsymbol{u}$. We can express any $1-$form $\boldsymbol{\alpha}$ in terms on basic $1-$forms as

$$\boldsymbol{\alpha} = \sum_{i=1}^n \alpha_i \boldsymbol{d}x^i \tag{2.5}$$

which means that the action of a $1-$form $\boldsymbol{\alpha}$ on a vector $\boldsymbol{u}$

$$\boldsymbol{\alpha}(\boldsymbol{u}) = \sum_{i=1}^n \alpha_i \boldsymbol{d}x^i(\boldsymbol{u}) = \sum_{i=1}^n \alpha_i u^i = \langle \boldsymbol{\alpha}, \boldsymbol{u} \rangle \in \mathbb{R} \tag{2.6}$$

is the component of the vector $\boldsymbol{u}$ in $\boldsymbol{\alpha}$ direction.

We know that two vectors $\boldsymbol{u}, \boldsymbol{v} \in \mathbb{R}^n$ form a parallelogram. The action of $\boldsymbol{d}x^1 \wedge \boldsymbol{d}x^2$ on the pair of vectors $\boldsymbol{u}$ and $\boldsymbol{v}$ is defined as follows

$$\begin{aligned} \boldsymbol{d}x^1 \wedge \boldsymbol{d}x^2(\boldsymbol{u}, \boldsymbol{v}) &= \boldsymbol{d}x^1(\boldsymbol{u})\boldsymbol{d}x^2(\boldsymbol{v}) - \boldsymbol{d}x^1(\boldsymbol{v})\boldsymbol{d}x^2(\boldsymbol{u}) \\ &= u^1 v^2 - v^1 u^2, \end{aligned} \tag{2.7}$$

which means that $\boldsymbol{d}x^1 \wedge \boldsymbol{d}x^2(\boldsymbol{u}, \boldsymbol{v})$ returns the area of the projection of the parallelogram onto x^1x^2-plane.Then, for two $1-$forms $\boldsymbol{\alpha}$, $\boldsymbol{\beta}$ we get

$$\boldsymbol{\alpha} \wedge \boldsymbol{\beta}(\boldsymbol{u}, \boldsymbol{v}) = \boldsymbol{\alpha}(\boldsymbol{u})\boldsymbol{\beta}(\boldsymbol{v}) - \boldsymbol{\alpha}(\boldsymbol{v})\boldsymbol{\beta}(\boldsymbol{u}). \tag{2.8}$$

By its definition, the wedge product is an antisymmetric product, which means

$$\boldsymbol{d}x^i \wedge \boldsymbol{d}x^j = -\boldsymbol{d}x^j \wedge \boldsymbol{d}x^i, \qquad i \neq j. \tag{2.9}$$

An inmediate result of (2.9) is $\boldsymbol{d}x^i \wedge \boldsymbol{d}x^i = 0$. It is important to notice that, by definition, the length of any built from the basic $1-$forms is one, i.e.

$$|\boldsymbol{d}x^1 \wedge \boldsymbol{d}x^2| = 1. \tag{2.10}$$

Now that we have a geometric interpretation for differential forms, we can see that if we take line integral of a vector field $\boldsymbol{u} = (u_i)$, where $i = 1, 2$, the integrand will take its general form as a linear combination of basic $1-$forms

$$\int u_1 \boldsymbol{d}x^1 + u_2 \boldsymbol{d}x^2, \tag{2.11}$$

which is equivalent to integrate the $1-$form $\boldsymbol{u}^\flat = u_1 \boldsymbol{d}x^1 + u_2 \boldsymbol{d}x^2$,

$$\int \boldsymbol{u}^\flat. \tag{2.12}$$

Similarly, for surface integrals

$$\int f(\boldsymbol{x}) dS = \int f \boldsymbol{d}x^1 \wedge \boldsymbol{d}x^2, \tag{2.13}$$

equivalent to the integration of the 2−form $f(\boldsymbol{x})\boldsymbol{d}x^1 \wedge \boldsymbol{d}x^2$.

The coefficients u_1, u_2 and $f(\boldsymbol{x})$ described in equations (2.11) and (2.13) are 0−forms.

The operator used in equation (2.12) is called the *flat* operator $\flat$ which gives a 1−form associated to a vector. Note that

$$\boldsymbol{u}^\flat(\boldsymbol{v}) = \langle \boldsymbol{u}, \boldsymbol{v} \rangle, \tag{2.14}$$

where $\boldsymbol{u}$ and $\boldsymbol{v}$ are vectors while $\boldsymbol{u}^\flat$ is the 1−form associated to $\boldsymbol{u}$.

Just as there is an operator that maps from vectors to 1−forms, there is also an operator mapping from 1−forms to vectors called the *sharp* operator $\sharp$ and if $\boldsymbol{\alpha} = \alpha_1 \boldsymbol{d}x^1 + \alpha_2 \boldsymbol{d}x^2$

$$\boldsymbol{\alpha}^\sharp = (\alpha_1, \alpha_2). \tag{2.15}$$

Thus $\boldsymbol{\alpha}^\sharp$ is the vector associated to $\boldsymbol{\alpha}$.

2.1.2 Hodge star

The main idea of the Hodge star of a form is to find a complementary form in order to obtain a multiple of the volume form in the given dimension. In 2 dimensions, considering the basic 1−forms $\{\boldsymbol{d}x^1, \boldsymbol{d}x^2\}$, by definition

$$\begin{aligned} \star \boldsymbol{d}x^1 &= \boldsymbol{d}x^2, \\ \star \boldsymbol{d}x^2 &= -\boldsymbol{d}x^1, \\ \star(\boldsymbol{d}x^1 \wedge \boldsymbol{d}x^2) &= = 1, \\ \star 1 &= \boldsymbol{d}x^1 \wedge \boldsymbol{d}x^2. \end{aligned}$$

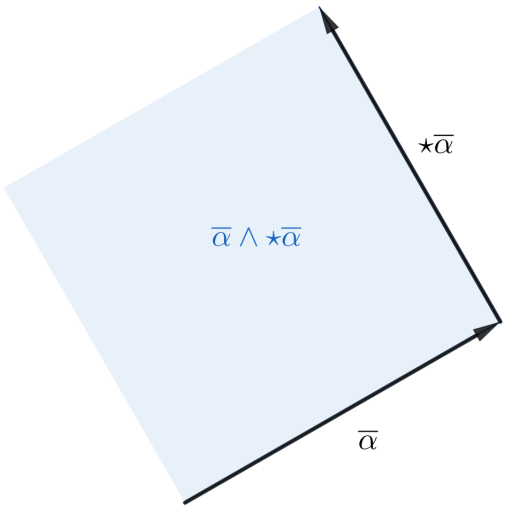

Figure 2.1: Geometric visualization for Hodge star

For a geometrical representation of Hodge star on $\mathbb{R}^2$, take $k = 1$, so that $\overline{\boldsymbol{\alpha}} \wedge \star\overline{\boldsymbol{\alpha}}$ must correspond to a square with side $|\overline{\boldsymbol{\alpha}}|$ as shown on figure 2.1.

In dimension 3,

$$\begin{aligned}
\star \boldsymbol{d}x^1 &= \boldsymbol{d}x^2 \wedge \boldsymbol{d}x^3, \\
\star \boldsymbol{d}x^2 &= \boldsymbol{d}x^3 \wedge \boldsymbol{d}x^1, \\
\star \boldsymbol{d}x^3 &= \boldsymbol{d}x^1 \wedge \boldsymbol{d}x^2, \\
\star(\boldsymbol{d}x^1 \wedge \boldsymbol{d}x^2) &= \boldsymbol{d}x^3, \\
\star(\boldsymbol{d}x^2 \wedge \boldsymbol{d}x^3) &= \boldsymbol{d}x^1, \\
\star(\boldsymbol{d}x^3 \wedge \boldsymbol{d}x^1) &= \boldsymbol{d}x^2, \\
\star(\boldsymbol{d}x^1 \wedge \boldsymbol{d}x^2 \wedge \boldsymbol{d}x^3) &= 1, \\
\star 1 &= \boldsymbol{d}x^1 \wedge \boldsymbol{d}x^2 \wedge \boldsymbol{d}x^3.
\end{aligned}$$

2.1.3 Exterior Derivative

Now, we will introduce the concept of *exterior derivative* in order to rewrite vector calculus operators using exterior calculus. In order to achieve that, we must consider $n = 3$ so that we can reproduce gradient, divergence and rotational operations.

In general, the exterior derivative $\boldsymbol{d}$ gives us information about how a $k-$form varies along any possible direction.

The exterior derivative of a function or $0-$form $f(\boldsymbol{x})$ is the $1-$form

$$\boldsymbol{d}f = \frac{\partial f}{\partial x^1}\boldsymbol{d}x^1 + \frac{\partial f}{\partial x^2}\boldsymbol{d}x^2 + \frac{\partial f}{\partial x^3}\boldsymbol{d}x^3. \tag{2.16}$$

We can recognize that (2.16) is equivalent to

$$\boldsymbol{d}f = (\boldsymbol{\nabla} f)^\flat \tag{2.17}$$

or equivalently

$$(\boldsymbol{d}f)^\sharp = \boldsymbol{\nabla} f.$$

Similarly, the exterior derivative of the $1-$form $\overline{\boldsymbol{u}} = u_1\boldsymbol{d}x^1 + u_2\boldsymbol{d}x^2 + u_3\boldsymbol{d}x^3$ will result in the $2-$form

$$\boldsymbol{d}\overline{\boldsymbol{u}} = \boldsymbol{d}(u_1\boldsymbol{d}x^1 + u_2\boldsymbol{d}x^2 + u_3\boldsymbol{d}x^3). \tag{2.18}$$

Since $\boldsymbol{d}$ is a linear operator, we get

$$\boldsymbol{d}\overline{\boldsymbol{u}} = \boldsymbol{d}(u_1\boldsymbol{d}x^1) + \boldsymbol{d}(u_2\boldsymbol{d}x^2) + \boldsymbol{d}(u_3\boldsymbol{d}x^3), \tag{2.19}$$

and rewriting $u_i\boldsymbol{d}x^i$ as the wedge product between a $0-$form and a $1-$form $u_i \wedge \boldsymbol{d}x^i$, then

$$\boldsymbol{d}\overline{\boldsymbol{u}} = \boldsymbol{d}(u_1 \wedge \boldsymbol{d}x^1) + \boldsymbol{d}(u_2 \wedge \boldsymbol{d}x^2) + \boldsymbol{d}(u_3 \wedge \boldsymbol{d}x^3), \tag{2.20}$$

using product rule

$$\boldsymbol{d}(u_i \wedge \boldsymbol{d}x^i) = \boldsymbol{d}u_i \wedge \boldsymbol{d}x^i + u_i \wedge \boldsymbol{d}\boldsymbol{d}x^i, \tag{2.21}$$

where $\boldsymbol{d}\boldsymbol{d}x^i = 0$, so that

$$\begin{aligned}\boldsymbol{d}\overline{\boldsymbol{u}} &= \boldsymbol{d}(u_1 \wedge \boldsymbol{d}x^1) + \boldsymbol{d}(u_2 \wedge \boldsymbol{d}x^2) + \boldsymbol{d}(u_3 \wedge \boldsymbol{d}x^3) \\ &= \boldsymbol{d}u_1 \wedge \boldsymbol{d}x^1 + \boldsymbol{d}u_2 \wedge \boldsymbol{d}x^2 + \boldsymbol{d}u_3 \wedge \boldsymbol{d}x^3,\end{aligned}$$

using (2.16) for u_1, u_2 and u_3

$$\begin{aligned}
\boldsymbol{d}\overline{\boldsymbol{u}} =& \boldsymbol{d}u_1 \wedge \boldsymbol{d}x^1 + \boldsymbol{d}u_2 \wedge \boldsymbol{d}x^2 + \boldsymbol{d}u_3 \wedge \boldsymbol{d}x^3 \\
=& \left(\frac{\partial u_1}{\partial x^1}\boldsymbol{d}x^1 + \frac{\partial u_1}{\partial x^2}\boldsymbol{d}x^2 + \frac{\partial u_1}{\partial x^3}\boldsymbol{d}x^3\right) \wedge \boldsymbol{d}x^1 \\
&+ \left(\frac{\partial u_2}{\partial x^1}\boldsymbol{d}x^1 + \frac{\partial u_2}{\partial x^2}\boldsymbol{d}x^2 + \frac{\partial u_2}{\partial x^3}\boldsymbol{d}x^3\right) \wedge \boldsymbol{d}x^2 \\
&+ \left(\frac{\partial u_3}{\partial x^1}\boldsymbol{d}x^1 + \frac{\partial u_3}{\partial x^2}\boldsymbol{d}x^2 + \frac{\partial u_3}{\partial x^3}\boldsymbol{d}x^3\right) \wedge \boldsymbol{d}x^3,
\end{aligned}$$

since wedge product is also linear, using antisymmetric property

$$\boldsymbol{d}x^i \wedge \boldsymbol{d}x^j = \begin{cases} -\boldsymbol{d}x^j \wedge \boldsymbol{d}x^i & i \neq j \\ 0 & i = j \end{cases}, \tag{2.22}$$

rearranging terms, we get

$$\boldsymbol{d}\overline{\boldsymbol{u}} = \left(\frac{\partial u_2}{\partial x^1} - \frac{\partial u_1}{\partial x^2}\right)\boldsymbol{d}x^1 \wedge \boldsymbol{d}x^2 + \left(\frac{\partial u_3}{\partial x^2} - \frac{\partial u_2}{\partial x^3}\right)\boldsymbol{d}x^2 \wedge \boldsymbol{d}x^3 + \left(\frac{\partial u_1}{\partial x^3} - \frac{\partial u_3}{\partial x^2}\right)\boldsymbol{d}x^3 \wedge \boldsymbol{d}x^1. \tag{2.23}$$

Summarizing, we have seen so far that exterior derivative maps $0-$forms to $1-$forms and $1-$forms to $2-$forms as shown in equations (2.16) and (2.23), respectively. If we continue with this procedure, eventually we will see that exterior derivative $\boldsymbol{d}$ maps $k-$forms to $(k+1)-$forms.

Now, we will obtain the equivalence for the curl of a vector field in vector calculus using exterior calculus by taking the dual of (2.23)

$$\star\, \boldsymbol{d}\overline{\boldsymbol{u}} = \left(\frac{\partial u_2}{\partial x^1} - \frac{\partial u_1}{\partial x^2}\right)\boldsymbol{d}x^3 + \left(\frac{\partial u_3}{\partial x^2} - \frac{\partial u_2}{\partial x^3}\right)\boldsymbol{d}x^1 + \left(\frac{\partial u_1}{\partial x^3} - \frac{\partial u_3}{\partial x^2}\right)\boldsymbol{d}x^2, \tag{2.24}$$

rearranging terms

$$\star\, \boldsymbol{d}\overline{\boldsymbol{u}} = \left(\frac{\partial u_3}{\partial x^2} - \frac{\partial u_2}{\partial x^3}\right)\boldsymbol{d}x^1 + \left(\frac{\partial u_1}{\partial x^3} - \frac{\partial u_3}{\partial x^1}\right)\boldsymbol{d}x^2 + \left(\frac{\partial u_2}{\partial x^1} - \frac{\partial u_1}{\partial x^2}\right)\boldsymbol{d}x^3, \tag{2.25}$$

and again, we can observe that

$$\star\, \boldsymbol{d}\overline{\boldsymbol{u}} \equiv \boldsymbol{\nabla} \times \boldsymbol{u}, \tag{2.26}$$

where $\boldsymbol{u} = (u_1, u_2, u_3)^T \in \mathbb{R}^3$.

In order to get the equivalence for the divergence with exterior calculus, we take the dual of $\overline{\boldsymbol{u}}$,

$$\star\, \overline{\boldsymbol{u}} = u_1 \boldsymbol{d}x^2 \wedge \boldsymbol{d}x^3 + u_2 \boldsymbol{d}x^3 \wedge \boldsymbol{d}x^1 + u_3 \boldsymbol{d}x^1 \wedge \boldsymbol{d}x^2, \tag{2.27}$$

now we take its exterior derivative and applying product rule, $\boldsymbol{d}\boldsymbol{d}x^i = 0$ for $i = 1, 2, 3$, the antisymmetric property for wedge product (2.22) and rearranging terms, we get

$$\boldsymbol{d} \star \overline{\boldsymbol{u}} = \left(\frac{\partial u_1}{\partial x^1} + \frac{\partial u_2}{\partial x^2} + \frac{\partial u_3}{\partial x^3} \right) \boldsymbol{d}x^1 \wedge \boldsymbol{d}x^2 \wedge \boldsymbol{d}x^3, \tag{2.28}$$

and taking its dual

$$\star\, \boldsymbol{d} \star \overline{\boldsymbol{u}} = \frac{\partial u_1}{\partial x^1} + \frac{\partial u_2}{\partial x^2} + \frac{\partial u_3}{\partial x^3}, \tag{2.29}$$

which is equal to a vector field divergence

$$\star\, \boldsymbol{d} \star \overline{\boldsymbol{u}} = \boldsymbol{\nabla} \cdot \boldsymbol{u}. \tag{2.30}$$

Finally, for the laplacian of a scalar field f, starting with its $1-$form $\boldsymbol{d}f$, we compute its dual

$$\star\, \boldsymbol{d}f = \frac{\partial f}{\partial x^1} \boldsymbol{d}x^2 \wedge \boldsymbol{d}x^3 + \frac{\partial f}{\partial x^2} \boldsymbol{d}x^3 \wedge \boldsymbol{d}x^1 + \frac{\partial f}{\partial x^3} \boldsymbol{d}x^1 \wedge \boldsymbol{d}x^2, \tag{2.31}$$

taking its exterior derivative, simplifying and rearranging terms

$$\boldsymbol{d} \star \boldsymbol{d}f = \left(\frac{\partial^2 f}{\partial (x^1)^2} + \frac{\partial^2 f}{\partial (x^2)^2} + \frac{\partial^2 f}{\partial (x^3)^2} \right) \boldsymbol{d}x^1 \wedge \boldsymbol{d}x^2 \wedge \boldsymbol{d}x^3, \tag{2.32}$$

we can see that its dual corresponds to the laplacian of f

$$\star\, \boldsymbol{d} \star \boldsymbol{d}f = \Delta f. \tag{2.33}$$

Now that we have found equivalences of vector calculus using dicrete calculus for basic operations, we can get equalities by using *flat* $\flat$ and *sharp* $\sharp$ operators, which means that our operations take

the form as follows

$$\boldsymbol{\nabla} f = (\boldsymbol{d}f)^{\sharp}, \tag{2.34a}$$

$$\Delta f = \star \boldsymbol{d} \star \boldsymbol{d} f, \tag{2.34b}$$

$$\boldsymbol{\nabla} \times \boldsymbol{u} = (\star \boldsymbol{d} \boldsymbol{u}^{\flat})^{\sharp}, \tag{2.34c}$$

$$\boldsymbol{\nabla} \cdot \boldsymbol{u} = \star \boldsymbol{d} \star \boldsymbol{u}^{\flat}. \tag{2.34d}$$

With these expressions we now need to understand the discrete version of exterior derivative $\boldsymbol{d}$ and Hodge star $\star$ in order to describe how DEC works.

2.1.4 Integration Theorems

In this section, we will review some integration theorems in vector calculus and rewrite them with exterior calculus so that we use Stokes' theorem for exterior calculus discretization.

Fundamental Theorem of Calculus

The fundamental theorem of calculus is stated as follows

Theorem 2.1.1 (Fundamental Theorem of Calculus)**.** *Let f be a real-valued function on a closed interval $[a, b]$ and F any antiderivative of f in (a, b), is f is Riemann integrable on (a, b), then*

$$\int_a^b f(x)dx = F(b) - F(a). \tag{2.35}$$

We can see that equation (2.35) corresponds to dimension $m = 1$ and that boundary operator ∂ acts on $1D$ domain $\Omega = [a, b]$ such that on the right side of the equation we are integrating over its boundary $\partial\Omega = a, b$ which corresponds to a $0D$ domain as shown in figure 2.2.

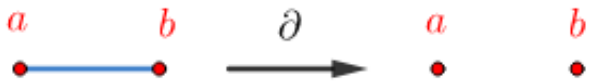

Figure 2.2: Boundary operator on $1D$ domain

If we define $F(x) = \omega(x)$ and $f(x) = \frac{\partial \omega}{\partial x}$, then equation (2.35) can be rewritten as

$$\int_{[a,b]} \frac{\partial \omega}{\partial x} \boldsymbol{d}x = \int_{\partial [a,b]} \omega. \tag{2.36}$$

Recall that scalar functions like ω are just $0-$forms and its derivative is given by equation (2.16), so once again, we can write

$$\int_{\Omega} \boldsymbol{d}\omega = \int_{\partial \Omega} \omega. \tag{2.37}$$

Green's theorem

Now, for surfaces ($2D$ manifolds) we know from vector calculus Green's theorem, which relates a double integral over a $2D$ domain Ω to a line integral over the boundary of the domain $\partial\Omega$, as it is stated below

Theorem 2.1.2 (Green's Theorem)**.** *Let C a positively oriented simple closed curve, D the region enclosed by C and $\boldsymbol{u} = (u_1, u_2)^T$ have continuous first order partial derivatives on D, then*

$$\int_D \left(\frac{\partial u_2}{\partial x} - \frac{\partial u_1}{\partial y} \right) dA = \int_C u_1 dx + u_2 dy. \tag{2.38}$$

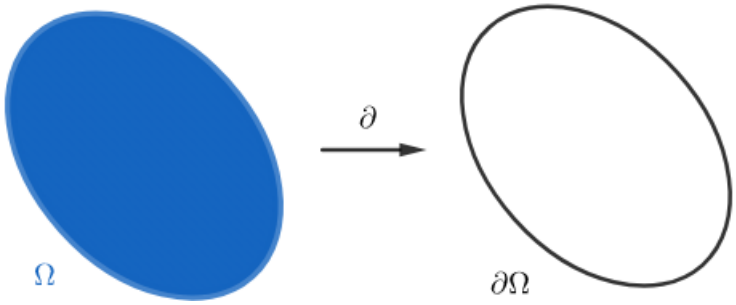

Figure 2.3: Boundary operator on $2D$ domain

As we previously pointed out, this is the case for $2D$ manifolds ($n = 2$), which means we may use $2D$ exterior calculus objects to rewrite (2.38). First we can identify, using the boundary operator ∂, $D = \Omega$ and $C = \partial\Omega$ for integration domains, as shown in figure 2.3, and $x = x^1$ and $y = x^2$ for cartesian coordinates, so we get

$$\int_{\Omega} \left(\frac{\partial u_2}{\partial x^1} - \frac{\partial u_1}{\partial x^2} \right) dA = \int_{\partial \Omega} u_1 dx^1 + u_2 dx^2. \tag{2.39}$$

Recall that $\omega = \boldsymbol{u}^\flat = u_1 \boldsymbol{d}x^1 + u_2 \boldsymbol{d}x^2$ is the $1-$form associated to vector field $\boldsymbol{u}$, its exterior derivative is given by equation (2.23), as we are working on $\mathbb{R}^2$ we must keep with just the first term, and the $2-$forms $dA = \boldsymbol{d}x^1 \wedge \boldsymbol{d}x^2$ so that we rewrite equation (2.39) as

$$\int_\Omega \boldsymbol{d}\omega = \int_{\partial\Omega} \omega. \tag{2.40}$$

Divergence Theorem

For case $n = 3$ we have the Divergence theorem, which relates surface integral of a vector field, which is called the *flux* through the surface, to the volume integral of the divergence over the region inside the surface.

Theorem 2.1.3 (Divergence theorem)**.** *Let V be a solid region and S is the boundary of V with positive orientation. Let $\boldsymbol{u}$ be a vector field whose components have continuous first order partial derivatives. Then,*

$$\int_V \boldsymbol{\nabla} \cdot \boldsymbol{u} dV = \int_S \boldsymbol{u} \cdot \hat{\boldsymbol{n}} dS, \tag{2.41}$$

where $\hat{\boldsymbol{n}}$ is the normal vector to S.

As we are considering a closed surface, we can split the surface integral on the right hand side as follows

$$\int_S \boldsymbol{u} \cdot \hat{\boldsymbol{n}} dS = \int_S \boldsymbol{u} \cdot \hat{\boldsymbol{n}}_3 \boldsymbol{d}x^1 \wedge \boldsymbol{d}x^2 + \boldsymbol{u} \cdot \hat{\boldsymbol{n}}_1 \boldsymbol{d}x^2 \wedge \boldsymbol{d}x^3 + \boldsymbol{u} \cdot \hat{\boldsymbol{n}}_2 \boldsymbol{d}x^3 \wedge \boldsymbol{d}x^1, \tag{2.42}$$

where $\hat{\boldsymbol{n}}_1 = (1,0,0)^T$, $\hat{\boldsymbol{n}}_2 = (0,1,0)^T$ and $\hat{\boldsymbol{n}}_3 = (0,0,1)^T$ because each direction is orthogonal to its respective $2-$form. This means that

$$\int_S \boldsymbol{u} \cdot \hat{\boldsymbol{n}} dS = \int_S u_3 \boldsymbol{d}x^1 \wedge \boldsymbol{d}x^2 + u_1 \boldsymbol{d}x^2 \wedge \boldsymbol{d}x^3 + u_2 \boldsymbol{d}x^3 \wedge \boldsymbol{d}x^1, \tag{2.43}$$

and we can recognize from (2.27)

$$\int_S \boldsymbol{u} \cdot \hat{\boldsymbol{n}} dS = \int_S \star \boldsymbol{u}^\flat. \tag{2.44}$$

As the Hodge star represents the orthogonal complement for any $k-$form on $\mathbb{R}^m$, it is no wonder the $2-$form $\star \boldsymbol{u}^\flat$ represents the orthogonal components on a surface of $1-$form $\boldsymbol{u}^\flat$. On the other

hand, we can see that volume integral takes the form

$$\int_V \boldsymbol{\nabla} \cdot \boldsymbol{u} dV = \int_V (\star \boldsymbol{d} \star \boldsymbol{u}^\flat) \boldsymbol{d}x^1 \wedge \boldsymbol{d}x^2 \wedge \boldsymbol{d}x^3 = \int_V \boldsymbol{d} \star \boldsymbol{u}^\flat, \tag{2.45}$$

thus, taking $\Omega = V$, $\partial\Omega = S$ and $\omega = \star \boldsymbol{u}^\flat$, divergence theorem is written as

$$\int_\Omega \boldsymbol{d}\omega = \int_{\partial\Omega} \omega. \tag{2.46}$$

Stokes' theorem

So far, we have seen integration theorems on 1, 2 and 3 dimentional spaces and we showed that each one of them can be expressed in the same way. This is because those integration theorems are particular cases of Stokes' theorem. This is quite an important result on differential geometry and an essential result for exterior calculus discretization, which is stated as

Theorem 2.1.4 (Stokes' theorem)**.** *Let ω a $(k-1)-$form, Ω a $k-$dimensional oriented manifold with $\partial\Omega$ its boundary, then*

$$\int_\Omega \boldsymbol{d}\omega = \int_{\partial\Omega} \omega. \tag{2.47}$$

This theorem will allow us to obtain discrete operators from differential operations, i.e. discrete exterior calculus.

Taking a similar notation as the inner product $\langle\langle \cdot, \cdot \rangle\rangle$ for integrals, we can rewrite (2.47) as

$$\langle\langle \boldsymbol{d}\omega, \Omega \rangle\rangle = \langle\langle \omega, \partial\Omega \rangle\rangle, \tag{2.48}$$

then, from

$$\langle \boldsymbol{A}\boldsymbol{a}, \boldsymbol{b} \rangle = \langle \boldsymbol{a}, \boldsymbol{A}^T \boldsymbol{b} \rangle, \tag{2.49}$$

where $\boldsymbol{A} \in \mathbb{R}^{d_1} \times \mathbb{R}^{d_2}$, $\boldsymbol{a} \in \mathbb{R}^{d_2}$ and $\boldsymbol{b} \in \mathbb{R}^{d_1}$, we can associate exterior derivative $\boldsymbol{d}$ with boundary operator as

$$\boldsymbol{d} = \partial^T. \tag{2.50}$$

2.2 Discrete Exterior Calculus

In the preceding section we reviewd the language of exterior calculus and its key concepts for DEC, such as the exterior derivative $\boldsymbol{d}$ and the Hodge star $\star$, and we showed some common operations in vector calculus using those elements. In this section we will build discrete versions of continuous operators so that we are able to express partial differential equations as a system of equations. In order to achieve this, we must describe the geometric objects needed for this theory.

2.2.1 Simple and Dual Meshes

When solving a PDE, we first need to define the domain Ω we are working on. Like other numerical methods, such as finite differences, finite volume, finite element, etc., DEC must discretize the domain. In particular, DEC does this by using a set of triangles, just like FEM when using triangular elements, which is constitutes a *simplicial complex*. From this mesh, called a *primal mesh*, we must define another discretization known as the *dual mesh* that comes from the use of Hodge star on elements from the primal mesh as shown in figure 2.4. One uses the circumcenters of the triangles to generate the dual edges.

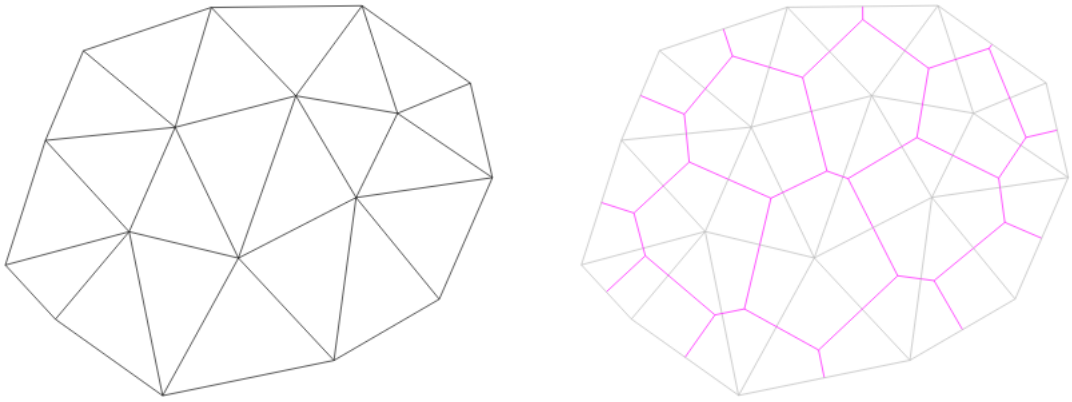

(a) Primal mesh (b) Dual mesh

Figure 2.4: Relationship between primal and dual meshes

2.2.2 Discrete Differential Forms

DEC performs operations on each positively oriented triangle (*2-simplex*) and its dual. From now on, we will be describing every 2−simplex as $[v_1, v_2, v_3]$ with local numeration, where $[v_1]$, $[v_2]$ and $[v_3]$ are its vertices (0−simplices) and $[v_1, v_2]$, $[v_2, v_3]$ and $[v_3, v_1]$ its oriented edges (1−simplices), it can be seen in figure 2.5.

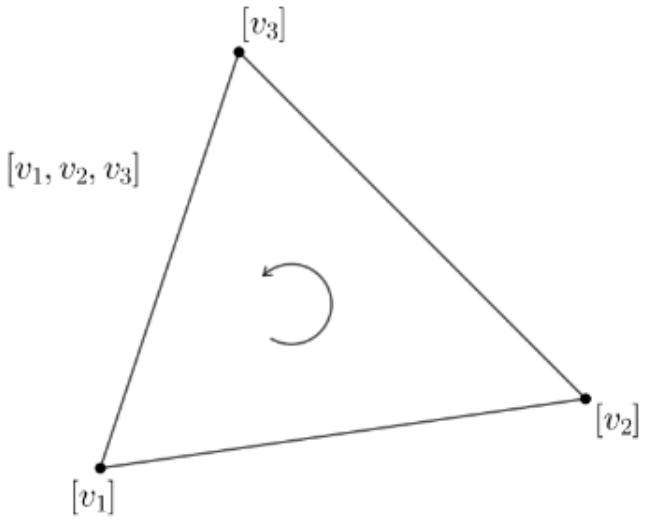

Figure 2.5: Simplex and its lower dimentional components

We know that each vertex is a 0−dimensional geometric object. The edges and the faces are 1-dimensional and 2−dimensional geometrical objects respectively. This allows us to discretize k−forms according to their dimensionality. For example, we can discretize 0−forms over vertices, 1−forms over edges and 2−forms over faces.

Let ϕ be a 0−form, then its discretization over a vertex $[v_i]$ is just an evaluation (integration) on the corresponding point $p_i = (x_i, y_i)$

$$\int_{[v_i]} \phi = \phi(p_i) = \phi_i, \qquad i = 1, 2, 3. \tag{2.51}$$

Thus, we get a vector

$$\phi \to \boldsymbol{\phi} = \begin{bmatrix} \phi_1 \\ \phi_2 \\ \phi_3 \end{bmatrix}. \tag{2.52}$$

2.2.3 Discrete Operators

So far, we have seen the discretizations of 0−forms and 1−forms. In this section, we will focus on discretizing the exterior calculus operators (on primal and dual meshes).

Discrete Exterior Derivative

Previously, we described how to discretize 1−forms such as $\boldsymbol{u}^\flat$. For 1−forms obtained as differentials of functions (0−forms) we can use Stokes' theorem as follows

$$(\boldsymbol{d}\phi)_{[v_i,v_j]} = \int_{[v_i,v_j]} \boldsymbol{d}\phi = \int_{\partial[v_i,v_j]} \phi = \int_{[v_i]}^{[v_j]} \phi = \phi_j - \phi_i, \qquad i,j = 1,2,3. \tag{2.53}$$

In 2 dimension, this allow us to get a matrix representation for the discrete exterior derivative operator on 0−forms

$$(\boldsymbol{d}\phi)_{[v_i,v_j]} \to \begin{bmatrix} \phi_2 - \phi_1 \\ \phi_3 - \phi_2 \\ \phi_1 - \phi_3 \end{bmatrix} = \begin{bmatrix} -1 & 1 & 0 \\ 0 & -1 & 1 \\ 1 & 0 & -1 \end{bmatrix} \begin{bmatrix} \phi_1 \\ \phi_2 \\ \phi_3 \end{bmatrix} = \boldsymbol{D}_{0,1}\boldsymbol{\phi}. \tag{2.54}$$

In general, the symbol $\boldsymbol{D}_{k,k+1}$ will represent the discrete exterior derivative mapping primal k−forms to primal $(k+1)$−forms.

We can also obtain $\boldsymbol{D}_{0,1}$ using the relationship $\boldsymbol{d} = \partial^T$, but we need to recall the definition of the boundary operator. For a $(k+1)$−simplex, the boundary operator is defined as follows

$$\partial_{k+1,k}[v_1, v_2, \ldots, v_k, v_{k+1}] = \sum_{j=1}^{k} (-1)^{j-1} [v_1, v_2, \ldots, \hat{v}_j, \ldots, v_k, v_{k+1}], \tag{2.55}$$

where $\hat{v}_j$ indicates that v_j is missing from the sequence.

Then taking the definition for boundary operator on 1−simplex we get

$$\partial[v_1, v_2] = [v_2] - [v_1], \tag{2.56a}$$

$$\partial[v_2, v_3] = [v_3] - [v_2], \tag{2.56b}$$

$$\partial[v_3, v_1] = [v_1] - [v_3], \tag{2.56c}$$

we can observe that

$$\partial[v_1, v_2] = -[v_1] + [v_2] + 0[v_3] = \begin{bmatrix}[v_1] & [v_2] & [v_3]\end{bmatrix} \begin{bmatrix}-1\\1\\0\end{bmatrix}, \tag{2.57a}$$

$$\partial[v_2, v_3] = 0[v_1] - [v_2] + [v_3] = \begin{bmatrix}[v_1] & [v_2] & [v_3]\end{bmatrix} \begin{bmatrix}0\\-1\\1\end{bmatrix}, \tag{2.57b}$$

$$\partial[v_3, v_1] = [v_1] + 0[v_2] - [v_3] = \begin{bmatrix}[v_1] & [v_2] & [v_3]\end{bmatrix} \begin{bmatrix}1\\0\\-1\end{bmatrix}, \tag{2.57c}$$

thus getting the matrix

$$\partial_{1,0} = \begin{bmatrix}-1 & 0 & 1\\1 & -1 & 0\\0 & 1 & -1\end{bmatrix}, \tag{2.58}$$

i.e.

$$\boldsymbol{D}_{0,1} = \partial_{1,0}^T = \begin{bmatrix}-1 & 1 & 0\\0 & -1 & 1\\1 & 0 & -1\end{bmatrix}. \tag{2.59}$$

The same procedure can be made to obtain $\boldsymbol{D}_{1,2}$ by applying $\partial_{2,1}$ to a $2-$simplex

$$\partial[v_1, v_2, v_3] = [v_2, v_3] - [v_1, v_3] + [v_1, v_2] = [v_1, v_2] + [v_2, v_3] + [v_3, v_1] \tag{2.60}$$

which means

$$\partial_{2,1} = \begin{bmatrix}1\\1\\1\end{bmatrix} \tag{2.61}$$

and

$$\boldsymbol{D}_{1,2} = \partial_{2,1}^{T} = \begin{bmatrix} 1 & 1 & 1 \end{bmatrix}. \tag{2.62}$$

Note that this matrix depends very much on the orientation of the $1-$simplices and the order in which we list them.

Discrete Hodge Star

As we mentioned at the beginning of 2.2, in order to define the discrete Hodge star operator, we must first define a dual mesh. Its elements must be orthogonal to their respective elements from the *primal mesh*. Just like in the definition of the *continuous* Hodge star, the action of discrete Hodge star operator on a $k-$dimentional element of a $n-$dimentional primal mesh will give a $(n-k)-$dimentional element on dual mesh.
In the case $n = 2$, for a given triangle we have

- Dual element of a primal $2-$simplex (triangle) $[v_1, v_2, v_3]$ corresponds on the circumcenter $[v_1, v_2, v_3]^*$ as shown in figure 2.6(a)
- Dual element of a primal $1-$simplex (edge) $[v_i, v_j]$ corresponds on the $[v_i, v_j]^*$ segment which is define as the oriented line that goes from the edge's middle point p_i to $[v_1, v_2, v_3]^*$ as can be seen in figure 2.6(b)
- Dual element of a primal $0-$simplex (vertex) $[v_i]$ corresponds on the quadrilateral $[v_i]^*$ which is positively oriented (counter-clockwise), formed by middle points of $[v_i]$ adjacent edges, circumcenter and $[v_i]$ showed in figure 2.6(c)

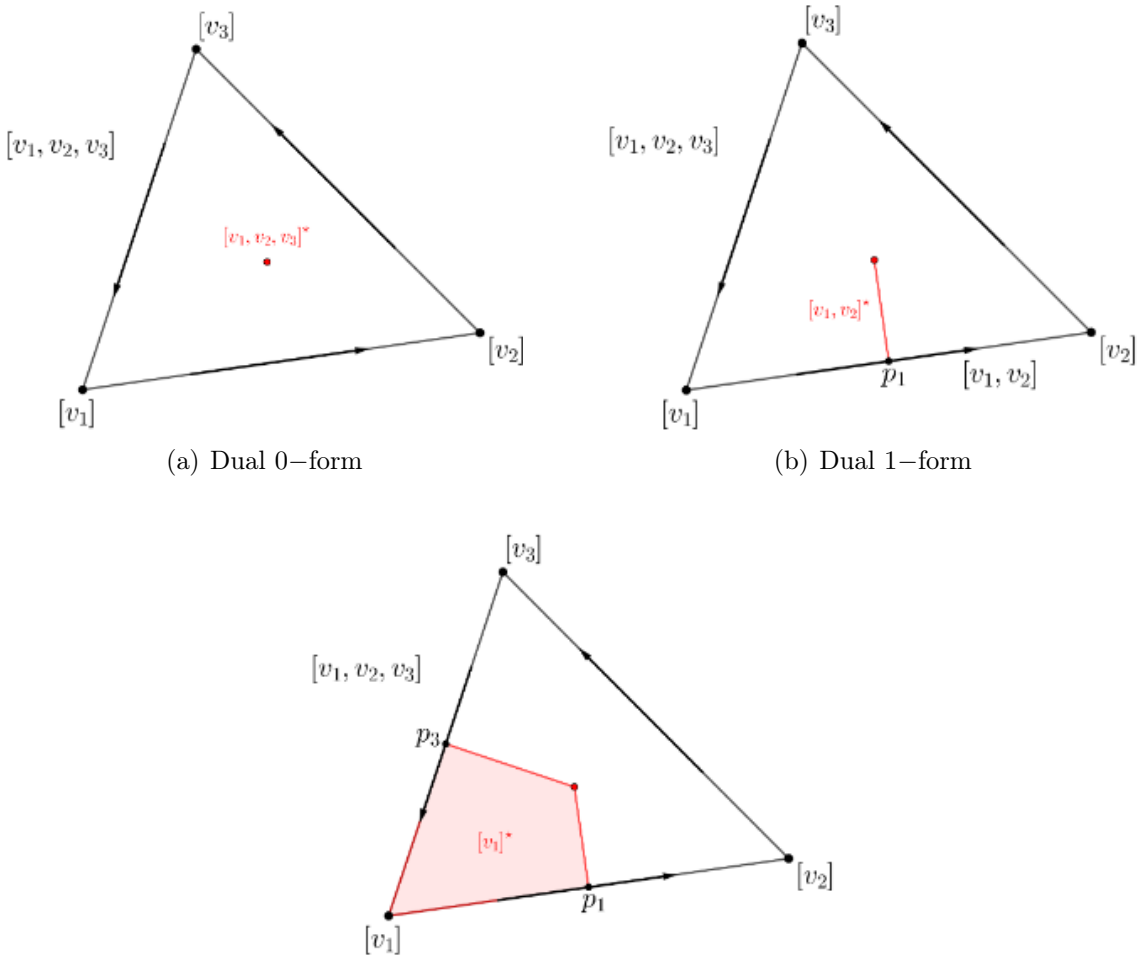

(a) Dual 0−form

(b) Dual 1−form

(c) Dual 2−form

Figure 2.6: Dual mesh elements

$k-$forms associated to the primal mesh are called *primal* $k-$*forms*, and those associated to the dual mesh are called *dual* $k-$*forms*. One type of discrete form can be transformed into the other by using the discrete Hodge star $\hat{\star}$, which is defined as follows

$$\int_{\sigma_k^*} \star\omega = \frac{|\sigma_k^*|}{|\sigma_k|} \int_{\sigma_k} \omega, \tag{2.63}$$

where the integration of the primal $k-$form ω over the primal $k-$simplex σ_k will give us the discretization for ω over σ_k, and similarly the integration of dual $k-$form $\star\omega$ over the dual $k-$simplex σ_k^*. As before, the symbol $|\cdot|$ denotes the length for the corresponding $k-$simplex or $k-$cell. In particular, the length of a vertex is defined to be equal to one, $|\sigma_0| = 1$.

We can see that when applying the discrete Hodge star, every primal $k-$form will be multiplied

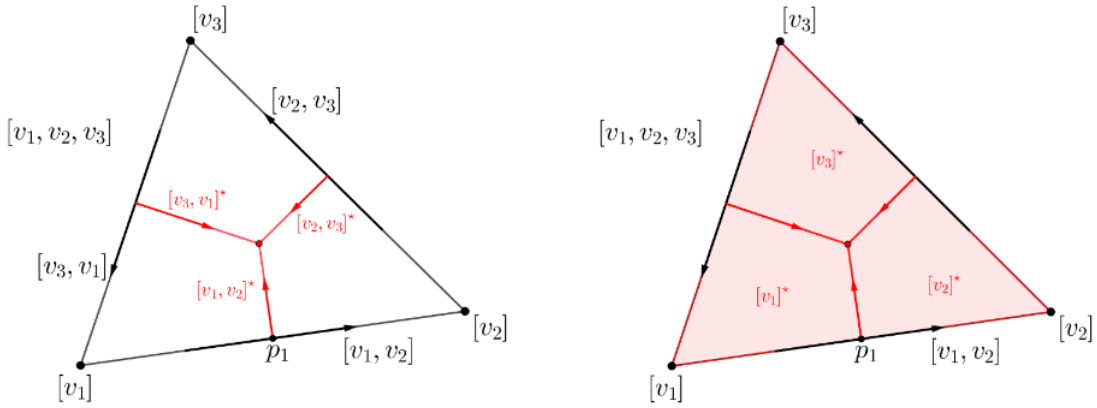

(a) Discrete primal 1−simplex and its dual (b) Discrete primal 0−simplex and its dual

Figure 2.7: Orientations of primal and dual mesh elements for $\boldsymbol{M}_{1,1}$ and $\boldsymbol{M}_{0,2}$

by a scalar, which means we will get a diagonal matrix that shall be denoted by $\boldsymbol{M}_{k,n-k}$, mapping discrete primal k−forms to dual $(n-k)$−forms.

In 2 dimensions, we can build the matrices $\boldsymbol{M}_{1,1}$ and $\boldsymbol{M}_{0,2}$

$$\boldsymbol{M}_{1,1} = \begin{bmatrix} \frac{|[v_1,v_2]|^*}{|[v_1,v_2]|} & 0 & 0 \\ 0 & \frac{|[v_2,v_3]|^*}{|[v_2,v_3]|} & 0 \\ 0 & 0 & \frac{|[v_3,v_1]|^*}{|[v_3,v_1]|} \end{bmatrix} \tag{2.64}$$

and

$$\boldsymbol{M}_{0,2} = \begin{bmatrix} \frac{|[v_1]|^*}{|[v_1]|} & 0 & 0 \\ 0 & \frac{|[v_2]|^*}{|[v_2]|} & 0 \\ 0 & 0 & \frac{|[v_3]|^*}{|[v_3]|} \end{bmatrix}, \tag{2.65}$$

respectively, this can be visualized in figure 2.7.

Discrete Dual Exterior Derivative

Now that we have defined dual $k-$cell and dual $k-$forms, we must also know how to operate on them. The Hodge star helps us by mapping primal $k-$forms to dual $k-$forms and viceversa, but we also need to know how the derivative acts on dual $k-$forms. Consider a dual $1-$form $\star\omega$ discretized over each dual $1-$simplex

$$\star\,\omega \rightarrow \begin{bmatrix} (\star\omega)_{[v_1,v_2]^*} \\ (\star\omega)_{[v_2,v_3]^*} \\ (\star\omega)_{[v_3,v_1]^*} \end{bmatrix}, \tag{2.66}$$

and by the given orientation shown in figure 2.7(b), we get

$$(d(\star\omega))_{[v_1,v_2]^*} = \int_{[v_1]^*} d(\star\omega) = \int_{\partial[v_1]^*} \star\omega = (\star\omega)_{[v_1,v_2]^*} - (\star\omega)_{[v_3,v_1]^*}, \tag{2.67a}$$

$$(d(\star\omega))_{[v_2,v_3]^*} = \int_{[v_2]^*} d(\star\omega) = \int_{\partial[v_2]^*} \star\omega = (\star\omega)_{[v_2,v_3]^*} - (\star\omega)_{[v_1,v_2]^*}, \tag{2.67b}$$

$$(d(\star\omega))_{[v_3,v_1]^*} = \int_{[v_3]^*} d(\star\omega) = \int_{\partial[v_3]^*} \star\omega = (\star\omega)_{[v_3,v_1]^*} - (\star\omega)_{[v_2,v_3]^*}, \tag{2.67c}$$

consequently, we can write discrete dual exterior derivative of a dual $1-$form with $\boldsymbol{D}^*_{1,2}$ matrix as

$$\boldsymbol{D}^*_{1,2} = \begin{bmatrix} 1 & 0 & -1 \\ -1 & 1 & 0 \\ 0 & -1 & 1 \end{bmatrix}. \tag{2.68}$$

In general, we will denote by $\boldsymbol{D}^*_{k,k+1}$ discrete dual exterior derivative operator, which maps dual $k-$forms to dual $(k+1)-$forms in $\mathbb{R}^n$.

We can see that $\boldsymbol{D}_{0,1}$ and $\boldsymbol{D}^*_{1,2}$ have the following relationship

$$\boldsymbol{D}^*_{1,2} = (-1)\boldsymbol{D}^T_{0,1}. \tag{2.69}$$

In fact, the general relationship for both discrete primal and dual exterior derivatives is given by (see [1])

$$\boldsymbol{D}^*_{(n-k),(n-k)+1} = (-1)^k \boldsymbol{D}^T_{k-1,k}. \tag{2.70}$$

Then, for $\boldsymbol{D}^*_{0,1}$ we get

$$\boldsymbol{D}^*_{0,1} = \boldsymbol{D}^T_{1,2} = \begin{bmatrix} 1 & 1 & 1 \end{bmatrix}, \tag{2.71}$$

as shown on Hirani's original work [1].

Now, we will focus on describing the transport equation in order to get its discretization by using the discrete operators described in this section.

2.3 The Transport Equation

In order to describe the transport equation, also called the convection-diffusion equation, we need to recall that the most fundamental law of physics is the law of energy conservation, which is such that for every branch of physics it has a different interpretation. For example, in thermodynamics it reads as follows

$$\frac{\partial \widetilde{\phi}}{\partial t} + \boldsymbol{\nabla} \cdot \boldsymbol{j} = 0, \tag{2.72}$$

where $\widetilde{\phi}$ is the volumetric density of heat and $\boldsymbol{j}$ is the heat flow. This tells us that the heat that flows outside a certain domain Ω must be the same as the variation of the heat density over time, i.e. heat is conserved.

The flux $\boldsymbol{j}$ can be divided into two terms: the convective and the diffusive terms $\boldsymbol{j} = \boldsymbol{j}_{\text{convection}} + \boldsymbol{j}_{\text{diffusion}}$. The convection term is the quantity of the transported field which moves across the boundaries because of the flow, and is proportional to the velocity field of the medium $\boldsymbol{u}$

$$\boldsymbol{j}_{\text{convection}} = \boldsymbol{u}\phi. \tag{2.73}$$

According to the second law of thermodynamics, heat is transferred from one body to another with lower thermal energy if there is an interaction between these two bodies by means of the diffusion

flux $\boldsymbol{j}_{\text{diffusion}}$, so that $\boldsymbol{j}_{\text{diffusion}}$ is porportional to the negative temperature gradient

$$\boldsymbol{j}_{\text{diffusion}} = -k\boldsymbol{\nabla}\phi, \tag{2.74}$$

where k is the thermal conductivity of the material and ϕ is the temperature of the material. On the other hand

$$\widetilde{\phi} = \rho c\phi, \tag{2.75}$$

where ρ is the material density and c is the specific heat of the material. Substituting (2.73), (2.74) and (2.75) in the continuity equation (2.72) and taking $\nu = \rho c$, we get

$$\frac{\partial(\nu\phi)}{\partial t} + \boldsymbol{\nabla}\cdot(\boldsymbol{u}\phi - k\boldsymbol{\nabla}\phi) = 0. \tag{2.76}$$

Consider an isotropic material (k constant) with constant material density and a specific heat constant over time (ν constant). We obtain

$$\nu\frac{\partial\phi}{\partial t} + \boldsymbol{\nabla}\cdot(\boldsymbol{u}\phi) - k\boldsymbol{\nabla}^2\phi = 0, \tag{2.77}$$

where $\boldsymbol{\nabla}^2 = \boldsymbol{\nabla}\cdot\boldsymbol{\nabla}$ is the Laplacian. As we mentioned before, equation (2.77) describes a temperature conservation. Nevertheless, the transport equation can be seen as a generalization for law of energy conservation due to the presence of a scalar source q. In the case we are analyzing, we will get the dynamic convection-diffusion equation

$$\nu\frac{\partial\phi}{\partial t} + \boldsymbol{\nabla}\cdot(\boldsymbol{u}\phi) - k\boldsymbol{\nabla}^2\phi = q. \tag{2.78}$$

Chapter 3

Methodology

In this chapter, we will discretize the dynamic transport equation using DEC and will make a comparision with FEM. We will also describe the cases where numerical instability must be taken into consideration and some techniques to deal with this issue. In particular, we use a correction scheme, which is our main contribution.

3.1 DEC Discretization for Transport Equation

Recall the dynamic transport equation (2.78)

$$\nu \frac{\partial \phi}{\partial t} + \boldsymbol{\nabla} \cdot (\boldsymbol{u}\phi) - k\boldsymbol{\nabla}^2 \phi = q. \tag{3.1}$$

First, we will focus on the discretization for source term q, diffusion term $-k\boldsymbol{\nabla}^2\phi$, convection term $\boldsymbol{\nabla} \cdot (\boldsymbol{u}\phi)$ and lastly the dynamic term $\nu \frac{\partial \phi}{\partial t}$.

3.1.1 Source Term Discretization

The discretization of the source term is quite straight forward as far as DEC is concerned, since we just have to discretize primal 0−form q on every primal 0−simplex σ_0 (vertex)

$$q \to \widetilde{\boldsymbol{q}} = \begin{bmatrix} q_1 \\ q_2 \\ q_3 \end{bmatrix}. \tag{3.2}$$

Later on, we will see that

$$\begin{aligned} \boldsymbol{q}_{DEC} =& \boldsymbol{M}_{0,2}\widetilde{\boldsymbol{q}} \\ =& \begin{bmatrix} \frac{|[v_1]^*|}{|[v_1]|} & 0 & 0 \\ 0 & \frac{|[v_2]^*|}{|[v_2]|} & 0 \\ 0 & 0 & \frac{|[v_3]^*|}{|[v_3]|} \end{bmatrix} \begin{bmatrix} q_1 \\ q_2 \\ q_3 \end{bmatrix} \\ =& \begin{bmatrix} \frac{|[v_1]^*|}{|[v_1]|} q_1 \\ \frac{|[v_2]^*|}{|[v_1]|} q_2 \\ \frac{|[v_3]^*|}{|[v_1]|} q_3 \end{bmatrix} \end{aligned} \tag{3.3}$$

is of greater interest for the source term discretization.

3.1.2 Diffusion Term Discretization

We must recall that the Laplacian of a scalar function (0−form) is expressed in exterior differential calculus as follows, $\boldsymbol{\nabla}^2\phi = \star\boldsymbol{d}\star\boldsymbol{d}\phi$. This means that we only have to replace each operator with its corresponding discrete operator. Consider the discretization of a primal 0−form ϕ on primal 0−simplices

$$\phi \to \boldsymbol{\phi} = \begin{bmatrix} \phi_1 \\ \phi_2 \\ \phi_3 \end{bmatrix}. \tag{3.4}$$

We can see that first exterior derivative maps from a primal 0−form to primal 1−form, meaning we must use $\boldsymbol{D}_{0,1}$

$$\boldsymbol{d}\phi \rightarrow \boldsymbol{D}_{0,1}\boldsymbol{\phi} = \begin{bmatrix} -1 & 1 & 0 \\ 0 & -1 & 1 \\ 1 & 0 & -1 \end{bmatrix} \begin{bmatrix} \phi_1 \\ \phi_2 \\ \phi_3 \end{bmatrix}. \tag{3.5}$$

Now, we see that the first Hodge star maps from a primal 1−form to dual 1−form, thus we use $\boldsymbol{M}_{1,1}$

$$\star\, \boldsymbol{d}\phi \rightarrow \boldsymbol{M}_{1,1}\boldsymbol{D}_{0,1}\boldsymbol{\phi} = \begin{bmatrix} -m_{1,2}^{(1)} & m_{1,2}^{(1)} & 0 \\ 0 & -m_{2,3}^{(1)} & m_{2,3}^{(1)} \\ m_{3,1}^{(1)} & 0 & -m_{3,1}^{(1)} \end{bmatrix} \begin{bmatrix} \phi_1 \\ \phi_2 \\ \phi_3 \end{bmatrix}, \tag{3.6}$$

where

$$m_{i,j}^{(1)} = \frac{|[v_i, v_j]^*|}{|[v_i, v_j]|}. \tag{3.7}$$

The second application of the exterior derivative now corresponds to mapping a dual 1−form to dual 2−form as follows

$$\boldsymbol{d} \star \boldsymbol{d}\phi \rightarrow \boldsymbol{D}_{1,2}^{*}\boldsymbol{M}_{1,1}\boldsymbol{D}_{0,1}\boldsymbol{\phi}, \tag{3.8}$$

using the relationship $\boldsymbol{D}_{1,2}^{*} = -\boldsymbol{D}_{0,1}^{T}$, we get

$$\begin{aligned} \boldsymbol{d} \star \boldsymbol{d}\phi &\rightarrow -\boldsymbol{D}_{0,1}^{T}\boldsymbol{M}_{1,1}\boldsymbol{D}_{0,1}\boldsymbol{\phi} \\ &= -\begin{bmatrix} m_{1,2}^{(1)} + m_{3,1}^{(1)} & -m_{1,2}^{(1)} & -m_{3,1}^{(1)} \\ -m_{1,2}^{(1)} & m_{1,2}^{(1)} + m_{2,3}^{(1)} & -m_{2,3}^{(1)} \\ m_{3,1}^{(1)} & -m_{2,3}^{(1)} & m_{2,3}^{(1)} + m_{3,1}^{(1)} \end{bmatrix} \begin{bmatrix} \phi_1 \\ \phi_2 \\ \phi_3 \end{bmatrix}. \end{aligned} \tag{3.9}$$

For further consideration, we take

$$\boldsymbol{K}_{DEC} = k\boldsymbol{D}_{0,1}^{T}\boldsymbol{M}_{1,1}\boldsymbol{D}_{0,1}. \tag{3.10}$$

Finally, the second Hodge star is replaced by $\boldsymbol{M}_{2,0}$ to map a dual 2−form into primal 0−form, which means that the discretized diffusion term is

$$-\boldsymbol{\nabla}^2\phi = -\star\, \boldsymbol{d} \star \boldsymbol{d}\phi \rightarrow -\boldsymbol{M}_{2,0}(-\boldsymbol{K}_{DEC})\boldsymbol{\phi} = \boldsymbol{M}_{2,0}\boldsymbol{K}_{DEC}\boldsymbol{\phi}. \tag{3.11}$$

Before writing its corresponding matrix components, consider Poisson equation (dynamic and convection terms are ignored from equation (2.78))

$$-k\boldsymbol{\nabla}^2\phi = q \qquad \rightarrow \qquad -\star\,\boldsymbol{d}\star\,\boldsymbol{d}\phi = q. \tag{3.12}$$

If we apply Hodge star we get

$$-\,\boldsymbol{d}\star\,\boldsymbol{d}\phi = \star q \tag{3.13}$$

and the $\star$ of the right hand side if replaced by the discrete operator $\boldsymbol{M}_{0,2}$. The system of equations obtained are

$$\boldsymbol{K}_{DEC}\boldsymbol{\phi} = \boldsymbol{q}_{DEC} \tag{3.14}$$

which is equivalent to

$$\boldsymbol{M}_{2,0}\boldsymbol{K}_{DEC}\boldsymbol{\phi} = \widetilde{\boldsymbol{q}} \tag{3.15}$$

due to the relationship

$$\boldsymbol{M}_{2,0} = \boldsymbol{M}_{0,2}^{-1}. \tag{3.16}$$

In order to keep working with the diffusion matrix $\boldsymbol{K}_{DEC}$ and the source vector $\boldsymbol{q}_{DEC}$, we will apply the Hodge star operator on the remaining terms of the dynamic transport equation, which will correspond to multiplying by $\boldsymbol{M}_{0,2}$ on the left.

3.1.3 Convection Term Discretization

The convection term $\boldsymbol{\nabla}\cdot(\boldsymbol{u}\phi)$ can be split into two terms by the product rule

$$\boldsymbol{\nabla}\cdot(\boldsymbol{u}\phi) = \boldsymbol{u}\cdot\boldsymbol{\nabla}\phi + (\boldsymbol{\nabla}\cdot\boldsymbol{u})\phi, \tag{3.17}$$

the first term on the right hand side corresponds to the directional derivative of ϕ on $\boldsymbol{u}$ direction and the second term corresponds to the velocity field divergence, whose physical meaning is the compresibility of the velocity field $\boldsymbol{u}$. We will discretize each term on its own as shown below.

Directional Derivative Discretization

First, we need to build directional derivative of ϕ on each edge direction. Considering primal $1-$simplex $[v_1]$ and recalling

$$(\boldsymbol{d}\phi)_{[v_i,v_j]} = \phi_j - \phi_i, \tag{3.18}$$

then, we take directional derivative of ϕ at $[v_1]$ on $[v_1, v_2]$ and $[v_3, v_1]$ directions and denoting by $\boldsymbol{w}_1$ as the gradient vector, then we get the system of equations

$$(\boldsymbol{p}_2 - \boldsymbol{p}_1) \cdot \boldsymbol{w}_1 = \phi_2 - \phi_1 \tag{3.19}$$

$$(\boldsymbol{p}_1 - \boldsymbol{p}_3) \cdot \boldsymbol{w}_1 = \phi_1 - \phi_3, \tag{3.20}$$

recall that $\boldsymbol{p}_i$ represents the vector associated to point p_i on $[v_i]$ vertex. Which results in

$$\boldsymbol{w}_1 = \frac{1}{2|[v_1, v_2, v_3]|} \begin{bmatrix} -(\boldsymbol{p}_3 - \boldsymbol{p}_2)_y\phi_1 - (\boldsymbol{p}_1 - \boldsymbol{p}_3)_y\phi_2 - (\boldsymbol{p}_2 - \boldsymbol{p}_1)_y\phi_3 \\ (\boldsymbol{p}_3 - \boldsymbol{p}_2)_x\phi_1 + (\boldsymbol{p}_1 - \boldsymbol{p}_3)_x\phi_2 + (\boldsymbol{p}_2 - \boldsymbol{p}_1)_x\phi_3 \end{bmatrix}, \tag{3.21}$$

where $(\boldsymbol{p}_j - \boldsymbol{p}_i)_x$ represents the x component of the vector $\boldsymbol{p}_j - \boldsymbol{p}_i$ and $(\boldsymbol{p}_j - \boldsymbol{p}_i)_y$ represents the y component of the same vector.

By repeating this procedure at $[v_2]$ and $[v_3]$ with their respective associated primal $1-$simplices for gradient vectors $\boldsymbol{w}_2$ and $\boldsymbol{w}_3$, respectively, we get

$$\boldsymbol{w}_1 = \boldsymbol{w}_2 = \boldsymbol{w}_3. \tag{3.22}$$

Taking the inner product of the gradient vector with the velocity vector field at each vertex, we get

$$\boldsymbol{u} \cdot \boldsymbol{\nabla}\varphi \to \boldsymbol{W}_1\boldsymbol{\varphi} = \begin{bmatrix} \boldsymbol{u}_1 \cdot \boldsymbol{w}_1 \\ \boldsymbol{u}_2 \cdot \boldsymbol{w}_2 \\ \boldsymbol{u}_3 \cdot \boldsymbol{w}_3 \end{bmatrix} = \frac{1}{|[v_1, v_2, v_3]|} \begin{bmatrix} \overline{\boldsymbol{u}}^1_{2,3} & \overline{\boldsymbol{u}}^1_{3,1} & \overline{\boldsymbol{u}}^1_{1,2} \\ \overline{\boldsymbol{u}}^2_{2,3} & \overline{\boldsymbol{u}}^2_{3,1} & \overline{\boldsymbol{u}}^2_{1,2} \\ \overline{\boldsymbol{u}}^3_{2,3} & \overline{\boldsymbol{u}}^3_{3,1} & \overline{\boldsymbol{u}}^3_{1,2} \end{bmatrix} \begin{bmatrix} \varphi_1 \\ \varphi_2 \\ \varphi_3 \end{bmatrix}, \tag{3.23}$$

where $\boldsymbol{u}_i = \boldsymbol{u}(p_i)$ and

$$\overline{\boldsymbol{u}}^k_{i,j} = \frac{1}{2}[-(\boldsymbol{u}_k)_x(\boldsymbol{p}_j - \boldsymbol{p}_i)_y + (\boldsymbol{u}_k)_y(\boldsymbol{p}_j - \boldsymbol{p}_i)_x. \tag{3.24}$$

The matrix associated to the directional derivative term is

$$\begin{aligned}\boldsymbol{U}^1_{DEC} &= \boldsymbol{M}_{0,2}\boldsymbol{W}_1 \\ &= \begin{bmatrix} \frac{|[v_1]^*|}{|[v_1,v_2,v_3]|}\overline{\boldsymbol{u}}^1_{2,3} & \frac{|[v_1]^*|}{|[v_1,v_2,v_3]|}\overline{\boldsymbol{u}}^1_{3,1} & \frac{|[v_1]^*|}{|[v_1,v_2,v_3]|}\overline{\boldsymbol{u}}^1_{1,2} \\ \frac{|[v_2]^*|}{|[v_1,v_2,v_3]|}\overline{\boldsymbol{u}}^2_{2,3} & \frac{|[v_2]^*|}{|[v_1,v_2,v_3]|}\overline{\boldsymbol{u}}^2_{3,1} & \frac{|[v_2]^*|}{|[v_1,v_2,v_3]|}\overline{\boldsymbol{u}}^2_{1,2} \\ \frac{|[v_3]^*|}{|[v_1,v_2,v_3]|}\overline{\boldsymbol{u}}^3_{2,3} & \frac{|[v_3]^*|}{|[v_1,v_2,v_3]|}\overline{\boldsymbol{u}}^3_{3,1} & \frac{|[v_3]^*|}{|[v_1,v_2,v_3]|}\overline{\boldsymbol{u}}^3_{1,2} \end{bmatrix}.\end{aligned} \tag{3.25}$$

Field Divergence discretization

The transport equation with incompressible flow has been studied in [6]. Here we propose a discretization for compressible flow given by the term $(\boldsymbol{\nabla}\cdot\boldsymbol{u})\phi$. In order to discretize this term we must observe that, unlike the directional derivative $\boldsymbol{u}\cdot\boldsymbol{\nabla}$, the differential operator $\boldsymbol{\nabla}\cdot$ acts on a known object $\boldsymbol{u}$, so that we can compute $\boldsymbol{\nabla}\cdot\boldsymbol{u}$ and consider it as a given function

$$f(x,y) = \boldsymbol{\nabla}\cdot\boldsymbol{u}, \tag{3.26}$$

which is a $0-$form. Thus, the discretization is

$$\begin{aligned}(\boldsymbol{\nabla}\cdot\boldsymbol{u})\phi \rightarrow & \begin{bmatrix} f_1\phi_1 \\ f_2\phi_2 \\ f_3\phi_3 \end{bmatrix} \\ &= \boldsymbol{W}_2\boldsymbol{\phi} \\ &= \begin{bmatrix} f_1 & 0 & 0 \\ 0 & f_2 & 0 \\ 0 & 0 & f_3 \end{bmatrix}\begin{bmatrix} \phi_1 \\ \phi_2 \\ \phi_3 \end{bmatrix}\end{aligned} \tag{3.27}$$

where $\{f_1, f_2, f_3\}$ is the discretization of f on the vertices. Thus, the matrix associated to velocity field divergence is

$$\begin{aligned}\boldsymbol{U}^2_{DEC} &= \boldsymbol{M}_{0,2}\boldsymbol{W}_2 \\ &= \begin{bmatrix} |[v_1]^*|f_1 & 0 & 0 \\ 0 & |[v_2]^*|f_2 & 0 \\ 0 & 0 & |[v_3]^*|f_3 \end{bmatrix}.\end{aligned} \tag{3.28}$$

We will be considering $\boldsymbol{U}_{DEC} = \boldsymbol{U}^1_{DEC} + \boldsymbol{U}^2_{DEC}$.

3.1.4 Dynamic Term Discretization

In order to get a discretization for the dynamic term, we can perform an Euler approximation

$$\frac{\partial \phi}{\partial t} \approx \frac{\phi^{t+1} - \phi^t}{\Delta t}, \tag{3.29}$$

where Δt is the time step size.

Taking the discretization of ϕ and multiplying by $\boldsymbol{M}_{0,2}$ on the left side, we get

$$\frac{\partial \phi}{\partial t} \to \frac{1}{\Delta t}\boldsymbol{M}_{0,2}\boldsymbol{\phi}^{t+1} - \frac{1}{\Delta t}\boldsymbol{M}_{0,2}\boldsymbol{\phi}^t. \tag{3.30}$$

3.2 Comparision with FEM

The Finite Element Method, FEM, allows us to solve PDEs numerically using different types of meshes of the doimain in which the equation of interest is defined. As its name reveals, this method focuses on performing computations on the elements composing the mesh by using a variational formulation with the help of interpolation functions. The case we are now interested is in $\mathbb{R}^2$. In this case FEM can use triangular or quadrilateral elements.

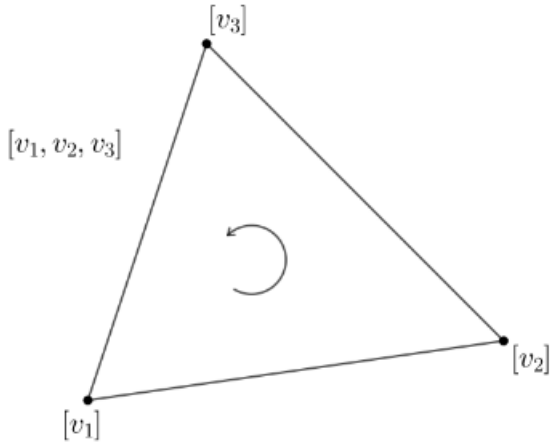

Figure 3.1: Linear triangular element

Since the discretization with DEC was formulated with a triangular mesh with three nodes (vertices) on each element, we will use the same element type and linear interpolation with FEM. In

order to make comparisions with both numerical methods, we will use the same notation we used in DEC.

Recall the positively oriented triangular elment shown in Figure 3.1. In order to compute the integral in the variational formulation, we just need to use Gauss quadrature. For a triangular linear element, we only need one integration point which corresponds to the triangle's barycenter Let

$$N_1(\varphi, \eta) = 1 - \varphi - \eta, \tag{3.31a}$$

$$N_2(\varphi, \eta) = \varphi, \tag{3.31b}$$

$$N_3(\varphi, \eta) = \eta, \tag{3.31c}$$

where

$$\varphi = \frac{1}{2|[v_1, v_2, v_3]|}[-(y_1 - y_3)x + (x_1 - x_3)y + x_2y_3 - x_3y_2], \tag{3.32a}$$

$$\eta = \frac{1}{2|[v_1, v_2, v_3]|}[-(y_2 - y_1)x + (x_2 - x_1)y + x_1y_2 - x_2y_1], \tag{3.32b}$$

and

$$x = \sum_{i=1}^{3} N_i x_i = (x_2 - x_1)\varphi + (x_3 - x_1)\eta + x_1, \tag{3.33a}$$

$$y = \sum_{i=1}^{3} N_i y_i = (y_2 - y_1)\varphi + (y_3 - y_1)\eta + y_1, \tag{3.33b}$$

Since Gauss quadrature and linear triangular elements are used, the only integration point is $(\varphi_G, \eta_G) = (1/3, 1/3)$ and its respective integration weight is $w_G = 1/2$, meaning

$$N_1(\varphi_G, \eta_G) = N_2(\varphi_G, \eta_G) = N_3(\varphi_G, \eta_G) = \frac{1}{3} \tag{3.34}$$

and

$$x_G = \sum_{i=1}^{3} N_i(\varphi_G, \eta_G)x_i = \frac{1}{3}\sum_{i=1}^{3} y_i = \overline{x}, \tag{3.35a}$$

$$y_G = \sum_{i=1}^{3} N_i(\varphi_G, \eta_G)y_i = \frac{1}{3}\sum_{i=1}^{3} y_i = \overline{y}. \tag{3.35b}$$

With this in mind, we will now proceed to the description of each term of the transport equation using the finite element method.

3.2.1 Source Term Discretization

The variational formulation for the source term q is given by

$$\int_{[v_1,v_2,v_3]} \boldsymbol{N_x} q_{\boldsymbol{x}} dxdy = \int_{\Omega} \boldsymbol{N_\varphi} q_{\boldsymbol{\varphi}} |\boldsymbol{J}| d\varphi d\eta, \tag{3.36}$$

where $|\boldsymbol{J}| = 2|[v_1, v_2, v_3]|$ is the determinant of jacobian matrix $\boldsymbol{J}$, Ω is the integration domain for local coordinates, the subscript $\boldsymbol{x}$ denotes functions using cartesian coordinates while the subscript $\boldsymbol{\varphi}$ denotes functions using local coordinates and N_i represents the $i-$th component of vector of interpolation functions

$$\boldsymbol{N} = \begin{bmatrix} N_1 \\ N_2 \\ N_3 \end{bmatrix}. \tag{3.37}$$

The source vector is

$$\boldsymbol{q}_{FEM} = \int_{\Omega} \boldsymbol{N_\varphi} q_{\boldsymbol{\varphi}} |\boldsymbol{J}| d\varphi d\eta. \tag{3.38}$$

As previously mentioned, the finite element method approximates the integral by using Gauss quadrature

$$\boldsymbol{q}_{FEM} \approx \boldsymbol{N}_G q_G |\boldsymbol{J}| w_G = \frac{|[v_1, v_2, v_3]|}{3} q_G \begin{bmatrix} 1 \\ 1 \\ 1 \end{bmatrix}, \tag{3.39}$$

where $q_G = q(\varphi_G, \eta_G)$ and $\boldsymbol{N}_G = \boldsymbol{N}(\varphi_G, \eta_G)$. Now, comparing with

$$\boldsymbol{q}_{DEC} = \begin{bmatrix} \frac{|[v_1]^*|}{|[v_1]|} q_1 \\ \frac{|[v_2]^*|}{|[v_1]|} q_2 \\ \frac{|[v_3]^*|}{|[v_1]|} q_3 \end{bmatrix}, \tag{3.40}$$

we can observe that if we use a constant source

$$q(\varphi, \eta) = q \tag{3.41}$$

and a equilateral triangle

$$|[v_1]^*| = |[v_2]^*| = |[v_3]^*| = \frac{|[v_1, v_2, v_3]|}{3}, \tag{3.42}$$

then $\boldsymbol{q}_{DEC} = \boldsymbol{q}_{FEM}$.

3.2.2 Diffusion Term Discretization

In this case, using the variational formulation and integration by parts we get the diffusion term

$$-k \int_{[v_1,v_2,v_3]} N_i \boldsymbol{\nabla}^2 \phi dxdy = k \int_{[v_1,v_2,v_3]} \boldsymbol{\nabla} N_i \cdot \boldsymbol{\nabla} \phi dxdy, \tag{3.43}$$

and we can write

$$\phi = \sum_{i=1}^{3} N_i \phi_i = \boldsymbol{N}^T \boldsymbol{\phi}, \tag{3.44}$$

which gives us the discrete diffusion term

$$-k\boldsymbol{\nabla}^2 \phi \to k \int_{[v_1,v_2,v_3]} \boldsymbol{\nabla N} \cdot \boldsymbol{\nabla N}^T dxdy \boldsymbol{\phi}, \tag{3.45}$$

this means our diffusion matrix is given by

$$\boldsymbol{K}_{FEM} = k \int_{[v_1,v_2,v_3]} \boldsymbol{\nabla N} \cdot \boldsymbol{\nabla N}^T dxdy \tag{3.46}$$

which is commonly written as

$$\boldsymbol{K}_{FEM} = \int_{[v_1,v_2,v_3]} \boldsymbol{B}^T \boldsymbol{D} \boldsymbol{B} dxdy. \tag{3.47}$$

It has been shown that $\boldsymbol{K}_{DEC} = \boldsymbol{K}_{FEM}$ (see [7]).

3.2.3 Convection Term Discretization

Just as with DEC, we will discretize directional derivative $\boldsymbol{u} \cdot \boldsymbol{\nabla}\phi$ and velocity field divergence $(\boldsymbol{\nabla} \cdot \boldsymbol{u})\phi$ terms on its own.

Directional Derivative Discretization

The variational formulation associated to this term is given by

$$\int_{[v_1,v_2,v_3]} \boldsymbol{N}(x,y)\boldsymbol{u}(x,y) \cdot \boldsymbol{\nabla}_{\boldsymbol{x}}\phi(x,y)dxdy = \int_{[v_1,v_2,v_3]} \boldsymbol{N}(x,y)\boldsymbol{u}(x,y) \cdot \boldsymbol{\nabla}_{\boldsymbol{x}}\phi(x,y)dxdy \tag{3.48}$$

where

$$\boldsymbol{\nabla}_{\boldsymbol{x}} = \begin{bmatrix} \frac{\partial}{\partial x} \\ \frac{\partial}{\partial y} \end{bmatrix} \qquad \text{and} \qquad \boldsymbol{\nabla}_{\boldsymbol{\varphi}} = \begin{bmatrix} \frac{\partial}{\partial \varphi} \\ \frac{\partial}{\partial \eta} \end{bmatrix} \tag{3.49}$$

are the gradients using cartesian and local coordinates, respectively. We get the relationship between $\boldsymbol{\nabla}_{\boldsymbol{x}}$ and $\boldsymbol{\nabla}_{\boldsymbol{\varphi}}$ using the chain rule

$$\boldsymbol{\nabla}_{\boldsymbol{x}} = \begin{bmatrix} \frac{\partial}{\partial x} \\ \frac{\partial}{\partial y} \end{bmatrix} = \begin{bmatrix} \frac{\partial \varphi}{\partial x}\frac{\partial}{\partial \varphi} + \frac{\partial \eta}{\partial x}\frac{\partial}{\partial \eta} \\ \frac{\partial \varphi}{\partial y}\frac{\partial}{\partial \varphi} + \frac{\partial \eta}{\partial y}\frac{\partial}{\partial \eta} \end{bmatrix} = \begin{bmatrix} \frac{\partial \varphi}{\partial x} & \frac{\partial \eta}{\partial x} \\ \frac{\partial \varphi}{\partial y} & \frac{\partial \eta}{\partial y} \end{bmatrix} \begin{bmatrix} \frac{\partial}{\partial \varphi} \\ \frac{\partial}{\partial \eta} \end{bmatrix} = \boldsymbol{J}^{-1}\boldsymbol{\nabla}_{\boldsymbol{\varphi}}. \tag{3.50}$$

Observe

$$\begin{aligned} \boldsymbol{u} \cdot \boldsymbol{\nabla}\phi &\to \int_{[v_1,v_2,v_3]} \boldsymbol{N}(x,y)\boldsymbol{u}(x,y) \cdot \boldsymbol{\nabla}_{\boldsymbol{x}}\phi(x,y)dxdy \\ &= \int_{[v_1,v_2,v_3]} \left(\boldsymbol{N}u_1\frac{\partial}{\partial x} + \boldsymbol{N}u_2\frac{\partial}{\partial y} \right) \phi dxdy \\ &= \int_{[v_1,v_2,v_3]} \begin{bmatrix} \boldsymbol{N} & \boldsymbol{N} \end{bmatrix} \begin{bmatrix} u_1 & 0 \\ 0 & u_2 \end{bmatrix} \boldsymbol{\nabla}_{\boldsymbol{x}}\phi dxdy. \end{aligned} \tag{3.51}$$

Replacing (3.50) and $\phi = \boldsymbol{N}^T\boldsymbol{\phi}$ on (3.51), we get

$$\begin{aligned}\boldsymbol{u}\cdot\boldsymbol{\nabla}\phi &\to \int_{[v_1,v_2,v_3]} \begin{bmatrix}\boldsymbol{N} & \boldsymbol{N}\end{bmatrix}\begin{bmatrix}u_1 & 0\\ 0 & u_2\end{bmatrix}\boldsymbol{\nabla}_{\boldsymbol{x}}\phi dxdy \\ &= \int_{\Omega}\begin{bmatrix}\boldsymbol{N} & \boldsymbol{N}\end{bmatrix}\begin{bmatrix}u_1 & 0\\ 0 & u_2\end{bmatrix}\boldsymbol{J}^{-1}\boldsymbol{\nabla}_{\boldsymbol{\varphi}}\boldsymbol{N}^T|\boldsymbol{J}|d\varphi d\eta\boldsymbol{\phi}.\end{aligned} \tag{3.52}$$

Thus, the matrix associated to directional derivative is

$$\boldsymbol{U}^1_{FEM} = \begin{bmatrix}\boldsymbol{N} & \boldsymbol{N}\end{bmatrix}\begin{bmatrix}u_1 & 0\\ 0 & u_2\end{bmatrix}\boldsymbol{J}^{-1}\boldsymbol{\nabla}_{\boldsymbol{\varphi}}\boldsymbol{N}^T|\boldsymbol{J}|d\varphi d\eta. \tag{3.53}$$

By using Gauss quadrature, we get the matrix

$$\begin{aligned}\boldsymbol{U}^1_{FEM} =& \int_{\Omega}\begin{bmatrix}\boldsymbol{N}_G & \boldsymbol{N}_G\end{bmatrix}\begin{bmatrix}u_1(\varphi_G,\eta_G) & 0\\ 0 & u_2(\varphi_G,\eta_G)\end{bmatrix}\boldsymbol{J}_G^{-1}(\boldsymbol{\nabla}_{\boldsymbol{\varphi}}\boldsymbol{N}^T)_G|\boldsymbol{J}|_G w_G \\ =&\frac{1}{3}\begin{bmatrix}\boldsymbol{u}_{2,3} & \boldsymbol{u}_{3,1} & \boldsymbol{u}_{1,2}\\ \boldsymbol{u}_{2,3} & \boldsymbol{u}_{3,1} & \boldsymbol{u}_{1,2}\\ \boldsymbol{u}_{2,3} & \boldsymbol{u}_{3,1} & \boldsymbol{u}_{1,2}\end{bmatrix},\end{aligned} \tag{3.54}$$

where

$$\boldsymbol{u}_{i,j} = \frac{1}{2}[-u_1(\overline{x},\overline{y})[v_i,v_j]_2 + u_2(\overline{x},\overline{y})[v_i,v_j]_1]. \tag{3.55}$$

Recall the convection matrix obtained with DEC

$$\boldsymbol{U}^1_{DEC} = \begin{bmatrix}\frac{|[v_1]^*|}{|[v_1,v_2,v_3]|}\overline{\boldsymbol{u}}^1_{2,3} & \frac{|[v_1]^*|}{|[v_1,v_2,v_3]|}\overline{\boldsymbol{u}}^1_{3,1} & \frac{|[v_1]^*|}{|[v_1,v_2,v_3]|}\overline{\boldsymbol{u}}^1_{1,2}\\ \frac{|[v_2]^*|}{|[v_1,v_2,v_3]|}\overline{\boldsymbol{u}}^2_{2,3} & \frac{|[v_2]^*|}{|[v_1,v_2,v_3]|}\overline{\boldsymbol{u}}^2_{3,1} & \frac{|[v_2]^*|}{|[v_1,v_2,v_3]|}\overline{\boldsymbol{u}}^2_{1,2}\\ \frac{|[v_3]^*|}{|[v_1,v_2,v_3]|}\overline{\boldsymbol{u}}^3_{2,3} & \frac{|[v_3]^*|}{|[v_1,v_2,v_3]|}\overline{\boldsymbol{u}}^3_{3,1} & \frac{|[v_3]^*|}{|[v_1,v_2,v_3]|}\overline{\boldsymbol{u}}^3_{1,2}\end{bmatrix}, \tag{3.56}$$

where

$$\overline{\boldsymbol{u}}^k_{i,j} = \frac{1}{2}[-(\boldsymbol{u}_k)_x(\boldsymbol{p}_j-\boldsymbol{p}_i)_y + (\boldsymbol{u}_k)_y(\boldsymbol{p}_j-\boldsymbol{p}_i)_x. \tag{3.57}$$

We can see that the differences between the FEM and DEC matrices lie in the factors 1/3 that appear in each entry of U_{FEM} as opposed to the factors $|[v_i]^*|/|[v_1, v_2, v_3]|$ and the evaluation of the velocity field at the average node, which corresponds to the barycenter of the triangle for FEM, or at each node according to the matrix input for DEC. This means that both matrices will be the same if $|[v_1]^*| = |[v_2]^*| = |[v_3]^*|$, i.e. the triangular element is a equilateral triangle and $\boldsymbol{u}$ is a constant velocity field.

Field Divergence Discretization

If $f(x, y) = \boldsymbol{\nabla} \cdot \boldsymbol{u}$, the variational formulation associated to this term is given by

$$(\boldsymbol{\nabla} \cdot \boldsymbol{u})\phi \to \int_{[v_1,v_2,v_3]} \boldsymbol{N} f \boldsymbol{N}^T dxdy\boldsymbol{\phi} = \int_{\Omega} f \boldsymbol{N}\boldsymbol{N}^T |\boldsymbol{J}| d\varphi d\eta \boldsymbol{\phi}, \tag{3.58}$$

which means the corresponding matrix is

$$\boldsymbol{U}^2_{FEM} = \int_{\Omega} f \boldsymbol{N}\boldsymbol{N}^T |\boldsymbol{J}| d\varphi d\eta \boldsymbol{\phi}. \tag{3.59}$$

Using Gauss quadrature and diagonalizing we get

$$\boldsymbol{U}^2_{FEM} = \frac{|[v_1, v_2, v_3]|}{3} f(\varphi_G, \eta_G)\boldsymbol{I} \tag{3.60}$$

and again, we will consider $\boldsymbol{U}_{FEM} = \boldsymbol{U}^1_{FEM} + \boldsymbol{U}^2_{FEM}$.
Comparing $\boldsymbol{U}^2_{DEC}$ and $\boldsymbol{U}^2_{FEM}$, we can see that if $|[v_1]^*| = |[v_2]^*| = |[v_3]^*|$, i.e. the triangular element is a equilateral triangle and there is a constant velocity field divergence $\boldsymbol{\nabla} \cdot \boldsymbol{u} = f$ =constant, then both matrices will be equal. Meaning that for $\boldsymbol{U}_{DEC} = \boldsymbol{U}_{FEM}$ we need $\boldsymbol{u}$ constant and the triangular element to be an equilateral triangle.

3.2.4 Dynamic Term Discretization

For this term, we must recall the Euler approximation algorithm. The variational formulation allows us to write

$$\begin{aligned}\frac{\partial \phi}{\partial t} \rightarrow & \frac{1}{\Delta t}\int_{[v_1,v_2,v_3]} \left(\boldsymbol{N}\phi^{t+1} - \boldsymbol{N}\phi^{t}\right) dxdy \\ = & \frac{1}{\Delta t}\int_{[v_1,v_2,v_3]} \boldsymbol{N}\boldsymbol{N}^T dxdy\boldsymbol{\phi}^{t+1} - \frac{1}{\Delta t}\int_{[v_1,v_2,v_3]} \boldsymbol{N}\boldsymbol{N}^T dxdy\boldsymbol{\phi}^{t}.\end{aligned} \tag{3.61}$$

We can observe the so called *mass matrix* $\hat{\boldsymbol{M}}_{FEM}$

$$\hat{\boldsymbol{M}}_{FEM} = \int_{[v_1,v_2,v_3]} \boldsymbol{N}\boldsymbol{N}^T dxdy. \tag{3.62}$$

By using Gauss quadrature and diagonalizing $\hat{\boldsymbol{M}}_{FEM}$, we get

$$\boldsymbol{M}_{FEM} = \begin{bmatrix} \frac{|[v_1,v_2,v_3]|}{3} & 0 & 0 \\ 0 & \frac{|[v_1,v_2,v_3]|}{3} & 0 \\ 0 & 0 & \frac{|[v_1,v_2,v_3]|}{3} \end{bmatrix} = \frac{|[v_1,v_2,v_3]|}{3}\boldsymbol{I}, \tag{3.63}$$

where $\boldsymbol{I} \in M_{3\times 3}(\mathbb{R})$ is the identity matrix. Again, we can see that if the triangular element is an equilateral triangle, then $\boldsymbol{M}_{0,2} = \boldsymbol{M}_{FEM}$.

3.3 Stabilization technique

In this section we will describe a technique used to deal with numerical instability on the convection-diffusion equation. The solution of this equation is often challenging because of the nature of the governing equation that lies on the convective and diffusion components.

3.3.1 Péclet number and numerical instability

The influence of both convection and diffusion effects are described by the Péclet number P_e, which is defined as

$$P_e = \frac{\text{convective transport rate}}{\text{diffusion transport rate}}. \tag{3.64}$$

When there is a large Péclet number $P_e > 1$, means there is convective dominance on the transport equation, while diffusion-dominated processes means we have a low Péclet number $P_e < 1$.
When attempting to solve convection-diffusion equation by discretizing it with any numerical method, it is common to observe oscillations in the computed solution. These oscillations may be due to physical phenomena or numerical instability. We can use the Péclet number to predict whether or not numerical instability will be present. For the convection-diffusion equation, Péclet is expressed as

$$P_e = \frac{|\overline{\boldsymbol{u}}|h}{2k}, \tag{3.65}$$

where $|\overline{\boldsymbol{u}}|$ is the magnitude of the mean velocity vector on the local element, k is the diffusion coefficient and h is the element's size, which may refer to the longest edge or the diameter of the circumsphere. If we are modeling a convection-dominated process $P_e > 1$, then we expect numerical instability to occur. There are several ways to deal with this situation. We will focus on two of them.

3.3.2 Artificial Diffusion and Correction Scheme

We can observe that convection dominance implies $|\overline{\boldsymbol{u}}|h > 2k$, which means that, in order to stabilize numerical solutions, we must decrease $|\overline{\boldsymbol{u}}|h$. We can only modify h, meaning we can decrease P_e by taking finer elements $h' < h$ with a finer mesh so that $|\overline{\boldsymbol{u}}|h > 2k > |\overline{\boldsymbol{u}}|h'$.
Consider adding an artificial diffusion component k_a on the static transport equation

$$\boldsymbol{\nabla} \cdot (\boldsymbol{u}\phi) - (k + k_a)\boldsymbol{\nabla}^2\phi = q, \tag{3.66}$$

such that $2k' = 2(k + k_a) > |\overline{\boldsymbol{u}}|h$ causing the numerical solution to not oscillate, nevertheless, this solution is not able to represent the original physical process. For this reason, we can come up with a technique able to remove the contribution of artificial diffusion to the stabilized solution, this technique is described below.

Discretizing equation (3.66) using any numerical method we get the stabilized system of equations

$$(\boldsymbol{K} + \boldsymbol{K}_a + \boldsymbol{U})\boldsymbol{\phi}_0 = \boldsymbol{q}, \tag{3.67}$$

where $\boldsymbol{K}$, $\boldsymbol{K}_a$ and $\boldsymbol{U}$ represent the matrices for diffusion, artificial diffusion and convection terms, respectively while $\boldsymbol{q}$ is the source vector and $\boldsymbol{\phi}_0$ the stabilized solution vector. In order to remove artificial diffusion, we must add the same contribution on the right hand side of the equation. Thus, we solve the system of equations

$$(\boldsymbol{K} + \boldsymbol{K}_a + \boldsymbol{U})\boldsymbol{\phi}_1 = \boldsymbol{q} + \boldsymbol{K}_a\boldsymbol{\phi}_0 \tag{3.68}$$

such that $\boldsymbol{\phi}_1$ is a stabilized solution with less contribution of artificial diffusion than $\boldsymbol{\phi}_0$.
We continue with this procedure

$$(\boldsymbol{K} + \boldsymbol{K}_a + \boldsymbol{U})\boldsymbol{\phi}_j = \boldsymbol{q} + \boldsymbol{K}_a\boldsymbol{\phi}_{j-1} \tag{3.69}$$

until

$$\frac{|\boldsymbol{\phi}_j - \boldsymbol{\phi}_{j-1}|}{|\boldsymbol{\phi}_j|} < \tau \tag{3.70}$$

holds, where τ is a tolerance error. This iterative algorithm is written below.

Algorithm 1 Static correction scheme for artificial diffusion

Require: $\boldsymbol{U}$, $\boldsymbol{K}$, $\boldsymbol{K}_a$, $\boldsymbol{q}$
Ensure: $\boldsymbol{\phi}_N = (\boldsymbol{K} + \boldsymbol{U})^{-1}\boldsymbol{q}$
1: $j \leftarrow 1$
2: $\tau_0 \leftarrow 1$
3: Solve $(\boldsymbol{K} + \boldsymbol{K}_a + \boldsymbol{U})\boldsymbol{\phi}_0 = \boldsymbol{q}$
4: **while** $|\tau_j| < \tau$ **do**
5: Solve $(\boldsymbol{K} + \boldsymbol{K}_a + \boldsymbol{U})\boldsymbol{\phi}_j = \boldsymbol{q} + \boldsymbol{K}_a\boldsymbol{\phi}_{j-1}$
6: $\tau_j \leftarrow |\boldsymbol{\phi}_j - \boldsymbol{\phi}_{j-1}|/|\boldsymbol{\phi}_j|$
7: $j \leftarrow j + 1$
8: **end while**

We can see that this static correction scheme, shown in equation (3.69), can be represented in the general form for an iterative algorithm as

$$\boldsymbol{\phi}_j = \boldsymbol{q}' + \boldsymbol{C}\boldsymbol{\phi}_{j-1} \tag{3.71}$$

where the constant vector and the iterative matrix are $\boldsymbol{q}' = \boldsymbol{B}^{-1}\boldsymbol{q}$ and $\boldsymbol{C} = \boldsymbol{B}^{-1}\boldsymbol{K}_a$, respectively. We know our algorithm converges when the spectral radius of the iterative matrix is lower than 1 $\rho(\boldsymbol{C}) < 1$. The spectral radius of a matrix $\boldsymbol{A}$ with eigenvalues $\{\lambda_i\}$ is defined as

$$\rho(\boldsymbol{A}) = \max\{|\lambda_i|\}. \tag{3.72}$$

In this case, if we define our artificial diffusion matrix as

$$\boldsymbol{K}_a = \delta\boldsymbol{K}, \quad \delta \in \mathbb{R}^+, \tag{3.73}$$

we can see that the δ parameter allows us to modify the eigenvalues for $\boldsymbol{C} = \frac{1}{\delta}\boldsymbol{B}^{-1}\boldsymbol{K}$.
On the other hand, we may ask, what exactly is happening when performing the previous algorithm? To answer this, we must recall, the main idea is

$$(\boldsymbol{U} + \boldsymbol{K})\boldsymbol{\phi}_j - \boldsymbol{q} \approx \boldsymbol{0} \tag{3.74}$$

for j large enough, where $\boldsymbol{Q} = \boldsymbol{B} - \boldsymbol{K}_a$ and $\boldsymbol{B} = \boldsymbol{U} + \boldsymbol{K} + \boldsymbol{K}_a$. By using (3.69), we can see what the actual result is

$$\begin{aligned} \boldsymbol{Q}\boldsymbol{\phi}_j - \boldsymbol{q} &= \boldsymbol{K}_a\boldsymbol{\phi}_{j-1} - \boldsymbol{K}_a\boldsymbol{\phi}_j \\ &= -\boldsymbol{K}_a(\boldsymbol{\phi}_j - \boldsymbol{\phi}_{j-1}) \end{aligned} \tag{3.75}$$

and observe that the term on the right-hand side corresponds to the numerator on the stopping criteria (3.70). This implies (3.75) will tend to zero, ensuring our algorithm will stop and remove the artificial diffusion contribution if (3.74) holds.

Since we must first solve

$$\boldsymbol{B}\boldsymbol{\phi}_0 = \boldsymbol{q} \tag{3.76}$$

then $\boldsymbol{B}$ has to be invertible, i.e. $\boldsymbol{B}^{-1}$ exists. This allows us to write the equation (3.69) as

$$\boldsymbol{\phi}_j = \boldsymbol{B}^{-1}\boldsymbol{q} + \boldsymbol{B}^{-1}\boldsymbol{K}_a\boldsymbol{\phi}_{j-1} \tag{3.77a}$$

and

$$\boldsymbol{\phi}_{j-1} = \boldsymbol{B}^{-1}\boldsymbol{q} + \boldsymbol{B}^{-1}\boldsymbol{K}_a\boldsymbol{\phi}_{j-2}. \tag{3.77b}$$

Replacing (3.77) in (3.75) we get

$$\begin{aligned} \boldsymbol{Q}\boldsymbol{\phi}_j - \boldsymbol{q} &= -\boldsymbol{K}_a(\boldsymbol{B}^{-1}\boldsymbol{K}_a\boldsymbol{\phi}_{j-1} - \boldsymbol{B}^{-1}\boldsymbol{K}_a\boldsymbol{\phi}_{j-2}) \\ &= -(\boldsymbol{K}_a\boldsymbol{B}^{-1})^1\boldsymbol{K}_a(\boldsymbol{\phi}_{j-1} - \boldsymbol{\phi}_{j-2}). \end{aligned} \tag{3.78}$$

Repeating this procedure $j-1$ times we will get

$$\boldsymbol{Q}\boldsymbol{\phi}_j - \boldsymbol{q} = -(\boldsymbol{K}_a\boldsymbol{B}^{-1})^j\boldsymbol{K}_a(\boldsymbol{\phi}_0 - \boldsymbol{\phi}_{-1}), \tag{3.79}$$

where $\boldsymbol{\phi}_{-1} = \boldsymbol{0}$. Finally, replacing (3.76) in (3.79)

$$\boldsymbol{Q}\boldsymbol{\phi}_j - \boldsymbol{q} = -(\boldsymbol{K}_a\boldsymbol{B}^{-1})^{j+1}\boldsymbol{q} = -\frac{1}{\delta^{j+1}}(\boldsymbol{K}\boldsymbol{B}^{-1})^{j+1}\boldsymbol{q}. \tag{3.80}$$

Let $\{\sigma_i\}$ and $\{\boldsymbol{w}_i\}$ be the eigenvalues and eigenvectors of $\boldsymbol{K}\boldsymbol{B}^{-1}$ respectively. Writting $\boldsymbol{q}$ as a linear combination of $\{\boldsymbol{w}_i\}$

$$\boldsymbol{q} = \sum_i \alpha_i \boldsymbol{w}_i \tag{3.81}$$

we can see

$$\begin{aligned} \boldsymbol{Q}\boldsymbol{\phi}_j - \boldsymbol{q} &= -\frac{1}{\delta^{j+1}}(\boldsymbol{K}\boldsymbol{B}^{-1})^{j+1}\boldsymbol{q} \\ &= -\frac{1}{\delta^{j+1}}(\boldsymbol{K}\boldsymbol{B}^{-1})^{j+1}\sum_i \alpha_i \boldsymbol{w}_i \\ &= -\sum_i \left(\frac{\lambda_i}{\delta}\right)^{j+1} \alpha_i \boldsymbol{w}_i. \end{aligned} \tag{3.82}$$

Thus, our algorithm achieves its purpose when $\max\{\lambda_i/\delta\} < 1$, which can be also achieved modifying the parameter δ.

We can apply the same idea for the dynamic transport equation

$$\nu\frac{\partial\phi}{\partial t} + \boldsymbol{\nabla}\cdot(\boldsymbol{u}\phi) - (k+k_a)\boldsymbol{\nabla}^2\phi = q, \tag{3.83}$$

with the system of equations

$$\left(\frac{\nu}{\Delta t}\boldsymbol{M} + \boldsymbol{K} + \boldsymbol{K}_a + \boldsymbol{U}\right)\boldsymbol{\phi}^{t+1} = \boldsymbol{q} + \frac{\nu}{\Delta t}\boldsymbol{M}\boldsymbol{\phi}^t, \tag{3.84}$$

where $t \in [0, T]$. Taking $\boldsymbol{B} = \boldsymbol{K} + \boldsymbol{K}_a + \boldsymbol{U}$ and $\boldsymbol{Q} = \boldsymbol{K} + \boldsymbol{U}$ then equation (3.84) can be written as

$$\left(\frac{\nu}{\Delta t}\boldsymbol{M} + \boldsymbol{B}\right)\boldsymbol{\phi}^{t+1} = \boldsymbol{q} + \frac{\nu}{\Delta t}\boldsymbol{M}\boldsymbol{\phi}^t. \tag{3.85}$$

We will perform an interpolation between solutions on two consecutive times t and $t+1$ using

$$\boldsymbol{B}\boldsymbol{\phi}^{t+1} \to \theta\boldsymbol{B}\boldsymbol{\phi}^{t+1} + (1-\theta)\boldsymbol{Q}\boldsymbol{\phi}^t, \tag{3.86}$$

where $\theta \in [0, 1]$, such that solutions are smooth between two consecutive times, i.e.

$$\left(\frac{\nu}{\Delta t}\boldsymbol{M} + \theta\boldsymbol{B}\right)\boldsymbol{\phi}_{t+1} = \boldsymbol{q} + \left[\frac{\nu}{\Delta t}\boldsymbol{M} - (1-\theta)\boldsymbol{Q}\right]\boldsymbol{\phi}_t. \tag{3.87}$$

By defining

$$\boldsymbol{A}(\theta) = \frac{\nu}{\Delta t}\boldsymbol{M} + \theta\boldsymbol{B}, \tag{3.88}$$

we get

$$\boldsymbol{A}(\theta)\boldsymbol{\phi}^{t+1} = [\boldsymbol{A}(\theta-1) + (1-\theta)\boldsymbol{K}_a]\boldsymbol{\phi}^t + \boldsymbol{q}, \tag{3.89}$$

meaning the dynamic correction scheme is written as

$$\boldsymbol{A}(\theta)\boldsymbol{\phi}^t_{j+1} = \boldsymbol{\psi}^t(\theta) + \boldsymbol{K}_a\boldsymbol{\phi}^t_j, \tag{3.90}$$

where

$$\boldsymbol{\psi}_j^t(\theta) = [\boldsymbol{A}(\theta - 1) + (1 - \theta)\boldsymbol{K}_a]\boldsymbol{\phi}_j^t + \boldsymbol{q}. \tag{3.91}$$

Recall $\boldsymbol{\phi}^0$ must be provided in order to compute $\boldsymbol{\phi}_0^1$ so that the static correction scheme is applied to get $\boldsymbol{\phi}_k^1$ solution with no contribution of artificial diffusion and we repeat this procedure on every time step $t \in [0, T]$.

The corresponding algorithm is written as

Algorithm 2 Dynamic correction scheme for artificial diffusion

Require: $\boldsymbol{U}$, $\boldsymbol{K}$, $\boldsymbol{K}_a$, $\boldsymbol{q}, \boldsymbol{\phi}^0, T, \theta$

$t \leftarrow 0$
while $t < T$ **do**
  Compute $\boldsymbol{\psi}_0^t(\theta) \leftarrow [\boldsymbol{A}(\theta - 1) + (1 - \theta)\boldsymbol{K}_a]\boldsymbol{\phi}_0^t + \boldsymbol{q}$
  $j \leftarrow 0$
  $\tau_j \leftarrow 1$
  while $\tau_j < \tau$ **do**
    Solve $\boldsymbol{A}(\theta)\boldsymbol{\phi}_{j+1}^t = \boldsymbol{\psi}_j^t(\theta) + \boldsymbol{K}_a\boldsymbol{\phi}_j^t$
    $\tau_j \leftarrow |\boldsymbol{\phi}_{j+1} - \boldsymbol{\phi}_j|/|\boldsymbol{\phi}_{j+1}|$
    $j \leftarrow j + 1$
  end while
  $t \leftarrow t + \Delta t$
end while

We can observe that this algorithm consists of applying the static correction scheme at every time step using $\boldsymbol{A}(\theta)$ instead of $\boldsymbol{B}$ and $\boldsymbol{\psi}^t$ instead of $\boldsymbol{q}$. Our convergence analysis also works for dynamic correction scheme.

Chapter 4

Numerical Examples

In this section we show the performance of DEC, as well as that of the stabilization technique described in the previous section, in three different numerical experiments for the transport equation.

4.1 Sinusoidal Velocity Field

For the first numerical example we consider a rectangular domain of dimentions 10×5 with its characteristics shown in figure 4.1, with the following configuration

- Diffusion coefficient $k = 0.05$
- Vector field $\boldsymbol{u}(x, y) = (x, \sin x)^T$
- Dynamic coefficient $\nu = 1$
- Initial value $\phi(0, x, y) = \phi_0 = 0$
- Final time $T = 5$
- Interpolation parameter $\theta = 0.6$

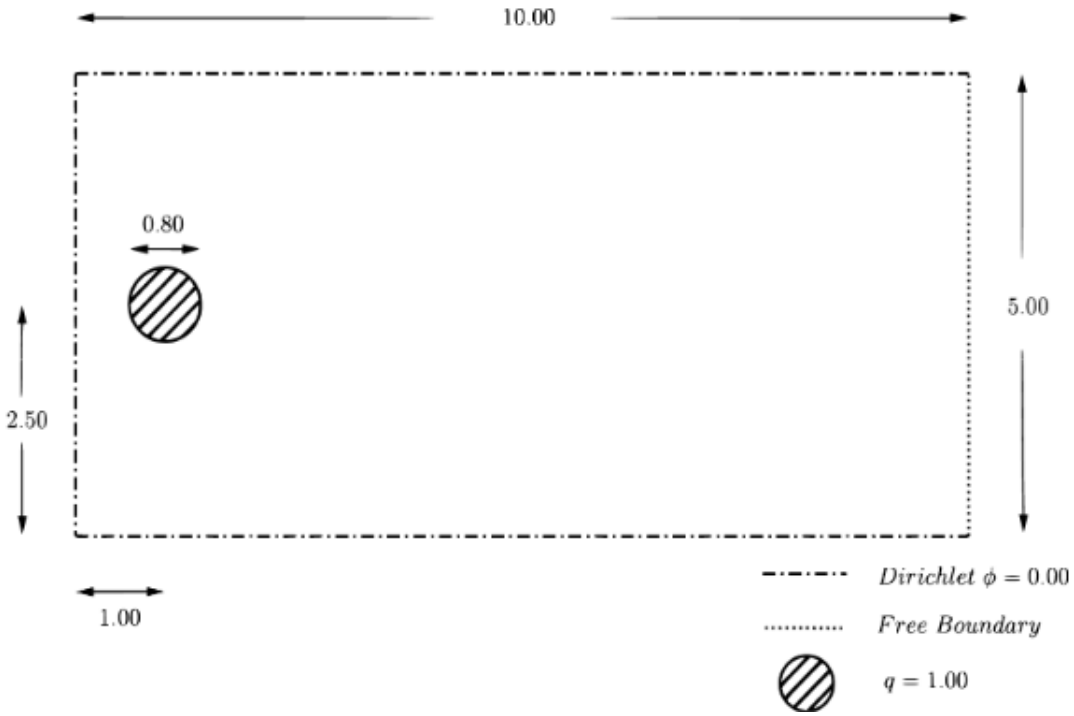

Figure 4.1: Rectangular domain and its characteristics for numerical experiments

When equilibrium has been reached, the static and the dynamic solutions must coincide, which means that in order to prove that the dynamic correction scheme works for both methods, we compared a static solution with a fine mesh (of $46,246$ elements) with the solution obtained from other three fine meshes, as shown in figure 4.2, in which we did use dynamic correction scheme with the following configuration

- Parameter for artificial diffusion $\delta = 20$
- Tolerance error $\tau = 10^{-10}$
- Maximum number of iterations $N = 10^4$ on each time step

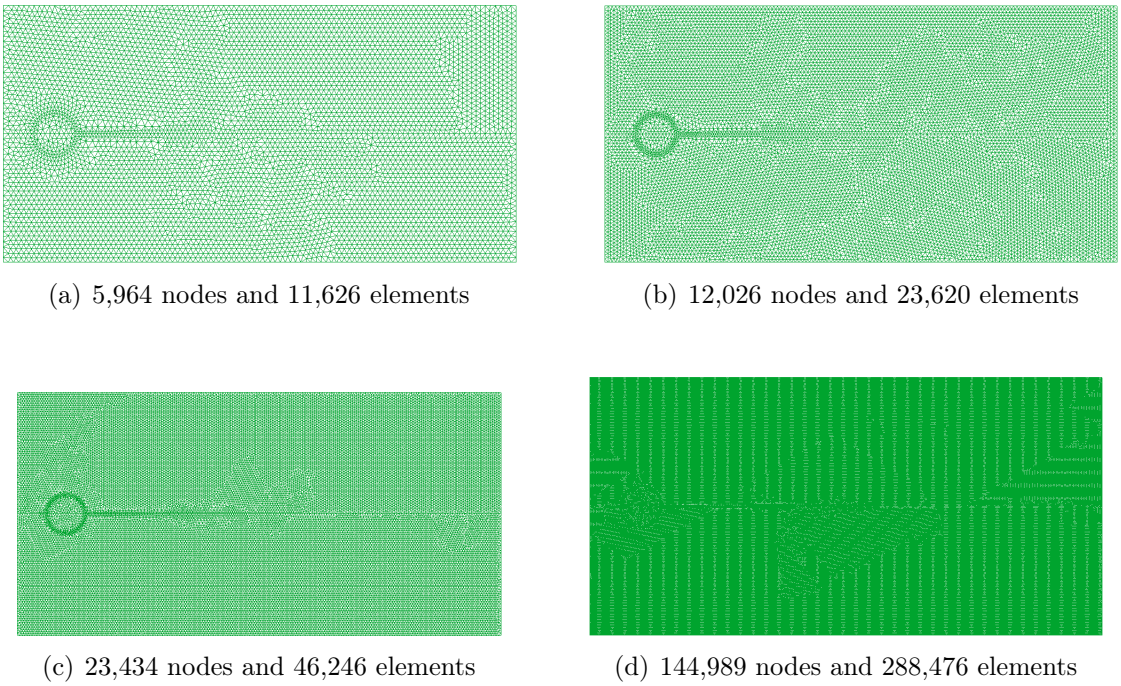

(a) 5,964 nodes and 11,626 elements

(b) 12,026 nodes and 23,620 elements

(c) 23,434 nodes and 46,246 elements

(d) 144,989 nodes and 288,476 elements

Figure 4.2: Fine meshes used for rectangular geometry

We plot the solutions obtained along the horizontal symmetric axis as shown in figure 4.3

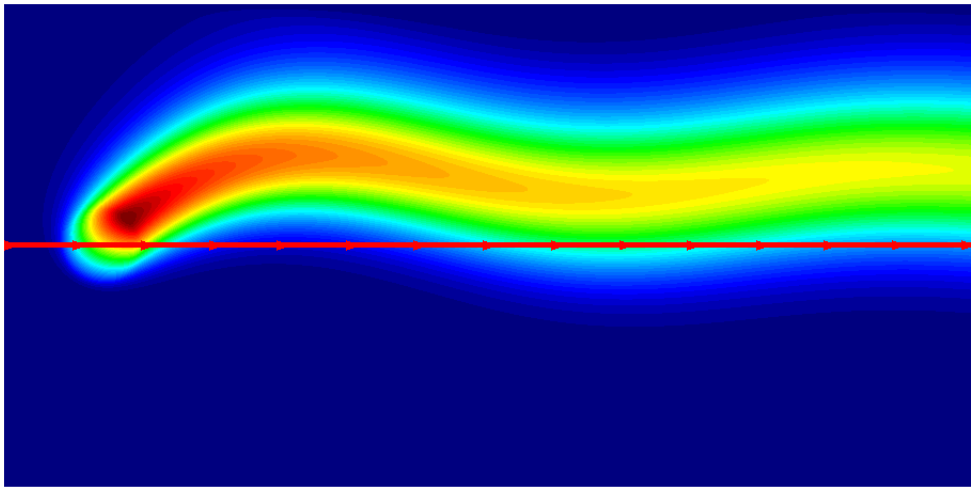

Figure 4.3: Static solution without correction scheme

We show in figure 4.4 the comparision for both methods with static and dynamic correction solutions using fine meshes.

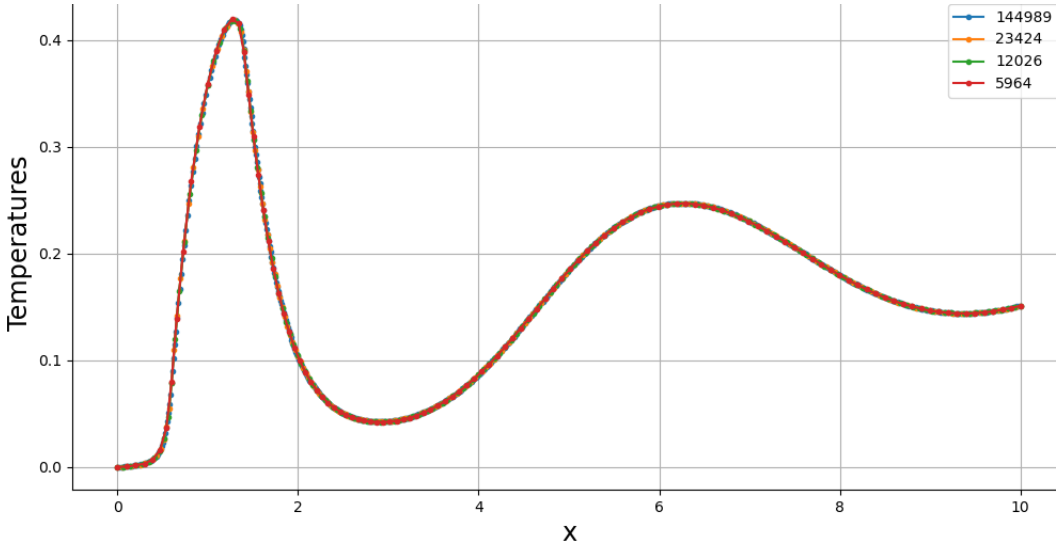

(a) Static and dynamic results using DEC

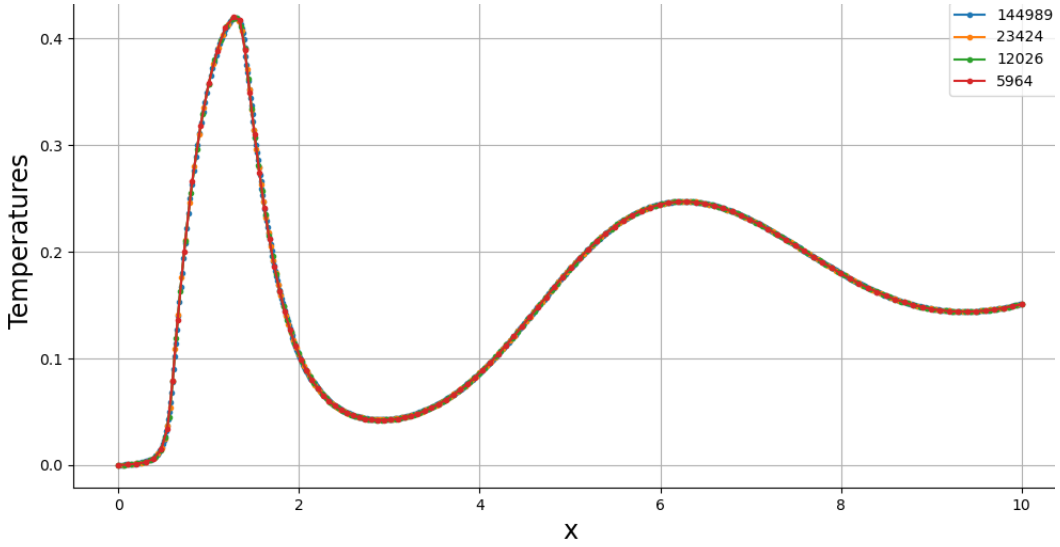

(b) Static and dynamic results using FEM

Figure 4.4: Solutions obtained from DEC and FEM for sinusoidal velocity

We can observe that the dynamic solutions obtained from both methods match the corresponding static solution, which means that the dynamic correction scheme is able to approximate the solution for the original equation by removing artificial diffusion at each time step.
We can see in Figures 4.5, 4.6 and 4.7 that the solutions from both methods behave similarly on each fine mesh. Nevertheless, we must have some measurements for better comparisions for these solutions.

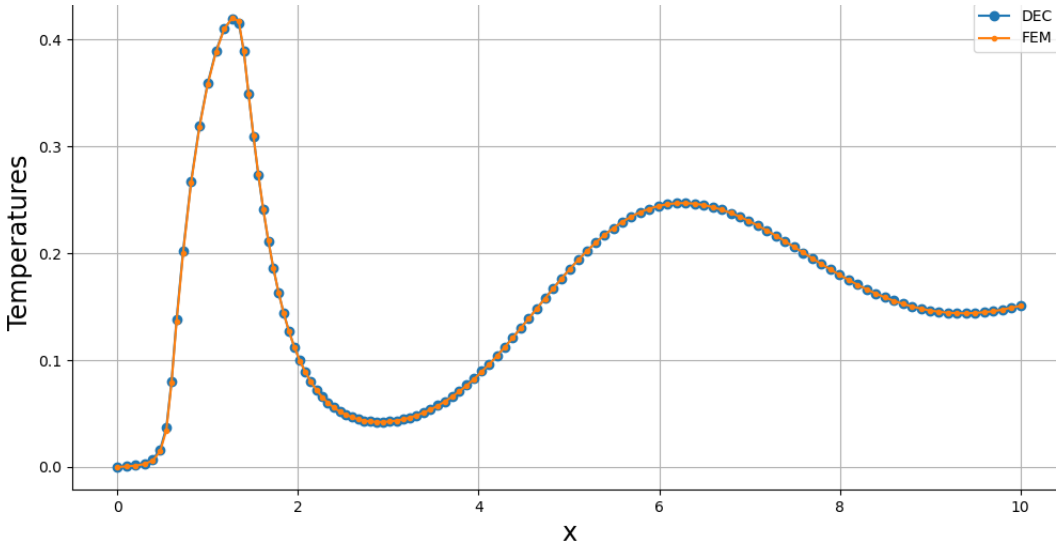

Figure 4.5: Comparision of dynamic solutions from methods on mesh 4.2(a)

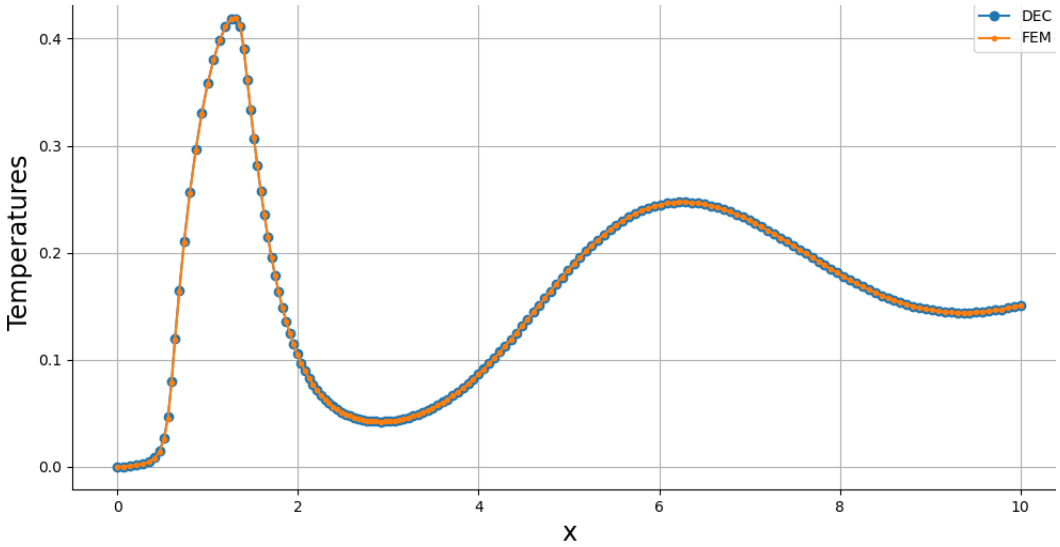

Figure 4.6: Comparision of dynamic solutions from methods on mesh 4.2(b)

For numerical comparisions, we must first define the *scaled error* between both methods as

$$\frac{|\phi_{DEC} - \phi_{FEM}|_2}{np}, \tag{4.1}$$

where np is the number of nodes on the horizontal axis and $|\cdot|_2$ denotes the L^2 norm. Recall that the cosine between two vectors is gien by

$$\frac{\langle \phi_{DEC}, \phi_{FEM} \rangle}{|\phi_{DEC}|_2 |\phi_{FEM}|_2}. \tag{4.2}$$

In table 4.1 we can see the comparisions with the previously described quantities for each mesh.

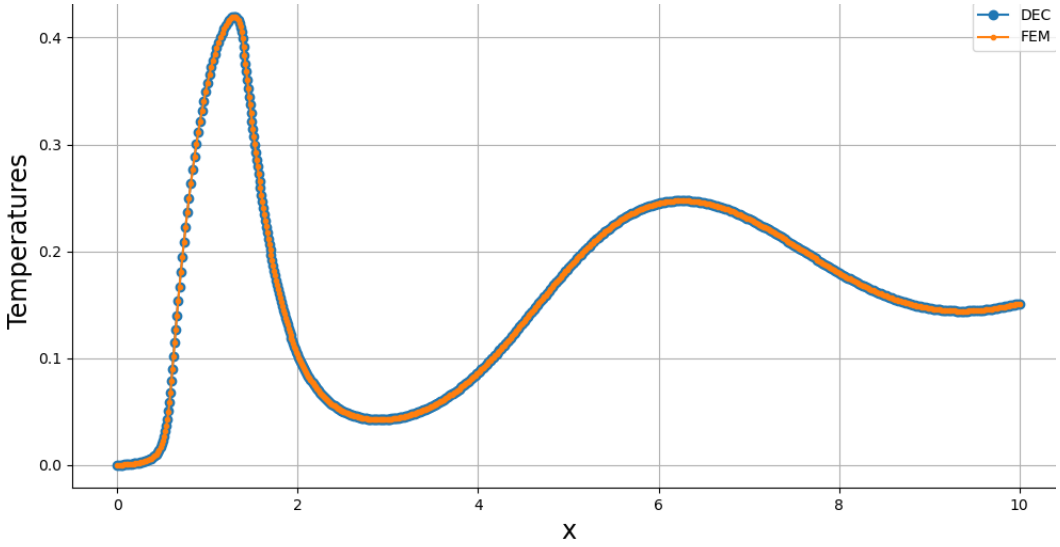

Figure 4.7: Comparision of dynamic solutions from methods on mesh 4.2(d)

Mesh	# Nodes	# Elements	Scaled error	Cosine
Fig. 4.2(a)	5,964	11,626	5.016398×10^{-5}	9.999957×10^{-1}
Fig. 4.2(b)	12,026	23,620	2.278808×10^{-5}	9.999987×10^{-1}
Fig. 4.2(d)	144,989	288,476	1.172347×10^{-6}	1.000000×10^{0}

Table 4.1: Comparision for dynamic solutions from both methods

It is easy to see that indeed both methods get quite similar results using the dynamic correction scheme for fine meshes.

We might also ask, what was the performance for each method as far as correction scheme is

concerned. For this reason, we show in figure 4.8 how many cumulative iterations were used for both DEC and FEM on each mesh.

We can observe that the finer the mesh, the more iterations are needed to converge regardless of the method used.

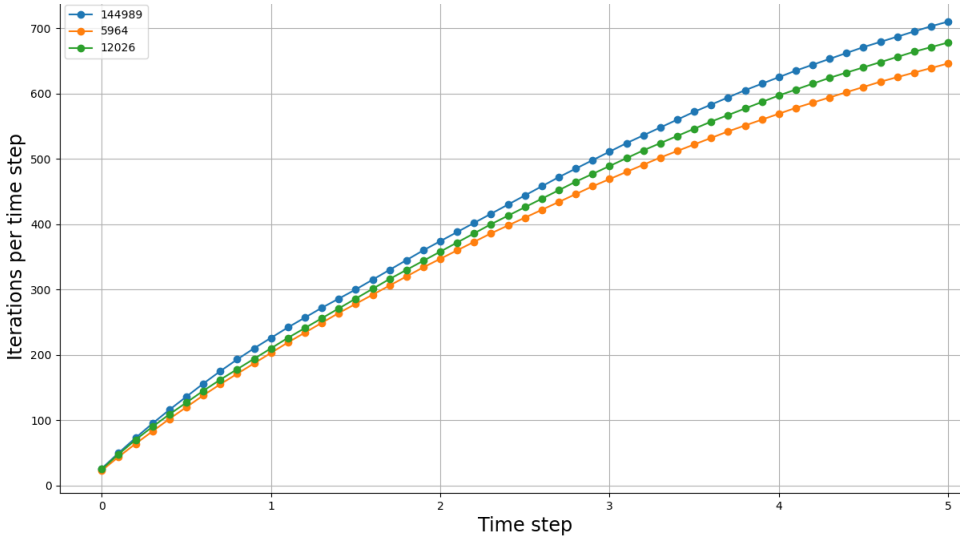

(a) DEC behavior on each fine mesh

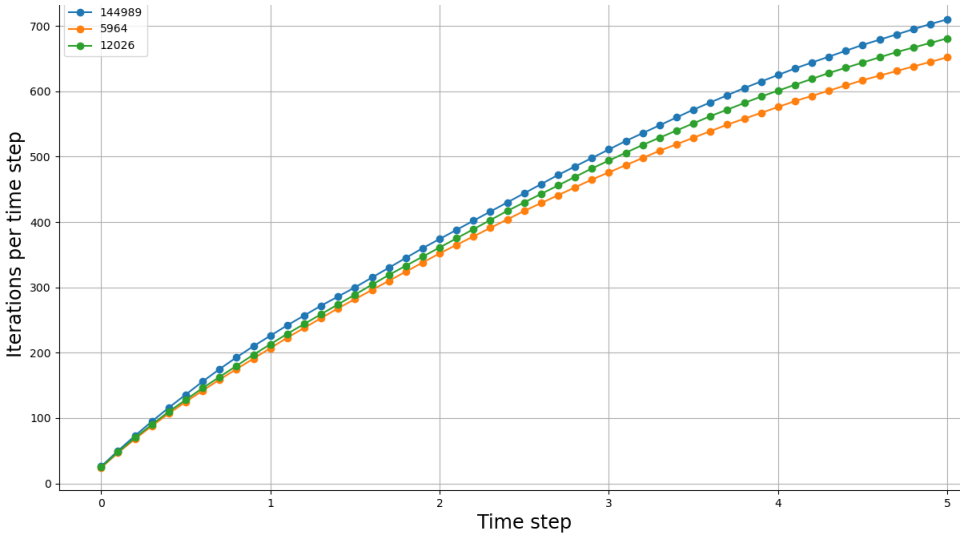

(b) FEM behavior on each fine mesh

Figure 4.8: Cumulative iterations per method

We show in figure 4.9 the performance of both methods on each fine mesh for cumulative iterations when using the dynamic correction scheme and we can observe DEC has a slightly better

performance, i.e. DEC needed less iterations than FEM, on each time step on every fine mesh as also shown in table 4.2 where we can observe that FEM used 282 and 167 more iterations than DEC on meshes 4.2(a) and 4.2(b) respectively.

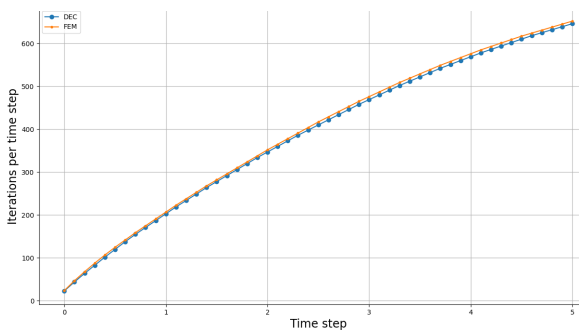

(a) Mesh 4.2(a)

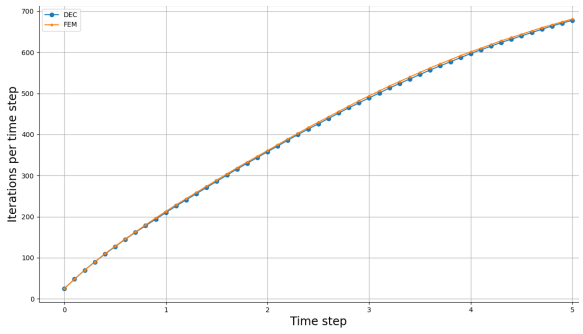

(b) Mesh 4.2(b)

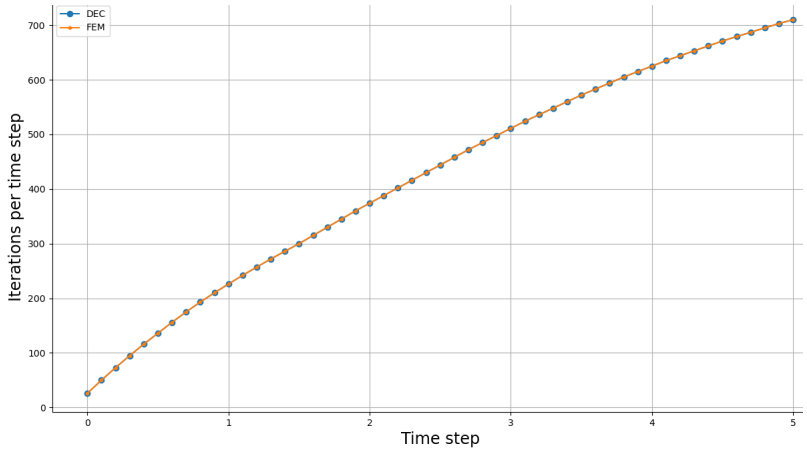

(c) Mesh 4.2(d)

Figure 4.9: Cumulative iterations per mesh

Mesh characteristics			Total iterations	
Mesh	# Nodes	# Elements	DEC	FEM
Fig. 4.2(a)	5,964	11,626	19,680	19,962
Fig. 4.2(b)	12,026	23,620	20,544	20,711
Fig. 4.2(d)	144,989	288,476	21,542	21,542

Table 4.2: Dynamic correction performance of both methods

Now that we know correction scheme works, we must compare the performance for both methods using coarse meshes so that the dynamic correction scheme must to be used. We will use the DEC solution for mesh 4.2(d) as the analytical approximation to compare with solutions for coarse

meshes shown in figure 4.10. We can observe that in the second set of meshes to use are so coarse

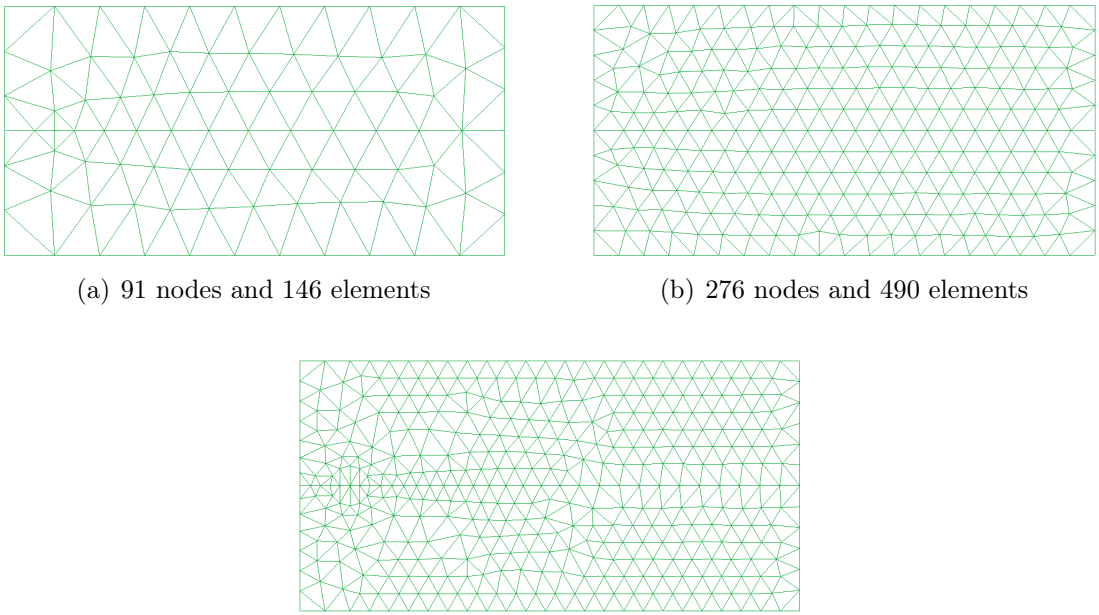

(a) 91 nodes and 146 elements

(b) 276 nodes and 490 elements

(c) 400 nodes and 722 elements

Figure 4.10: Coarse meshes used for rectangular geometry

that on its finest mesh we can barely distinguish the source term disk on the rectangular domain. In figures 4.11, 4.12 and 4.13 are shown the results obtained on coarse meshes from both methods.

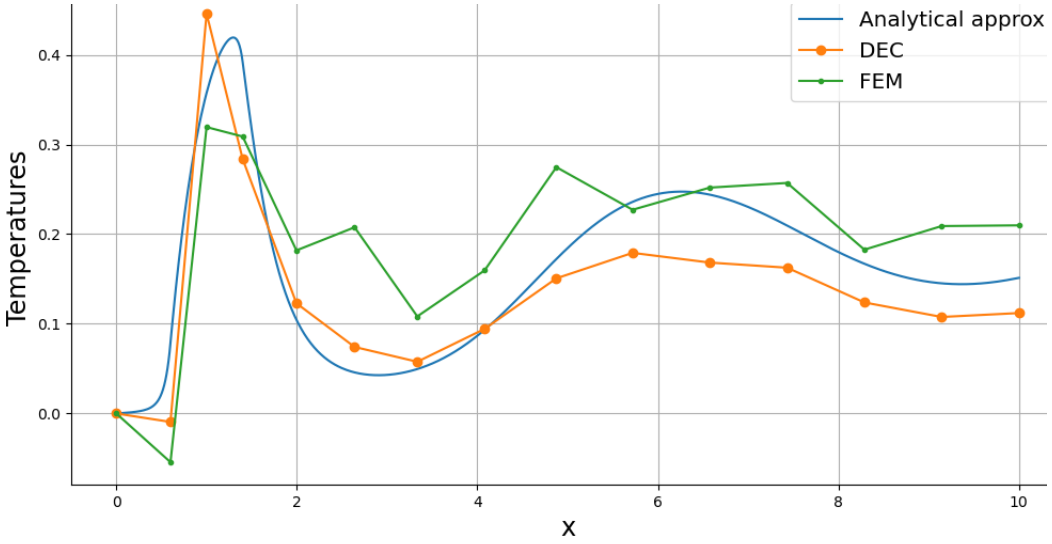

Figure 4.11: Comparision of dynamic solutions on mesh 4.10(a)

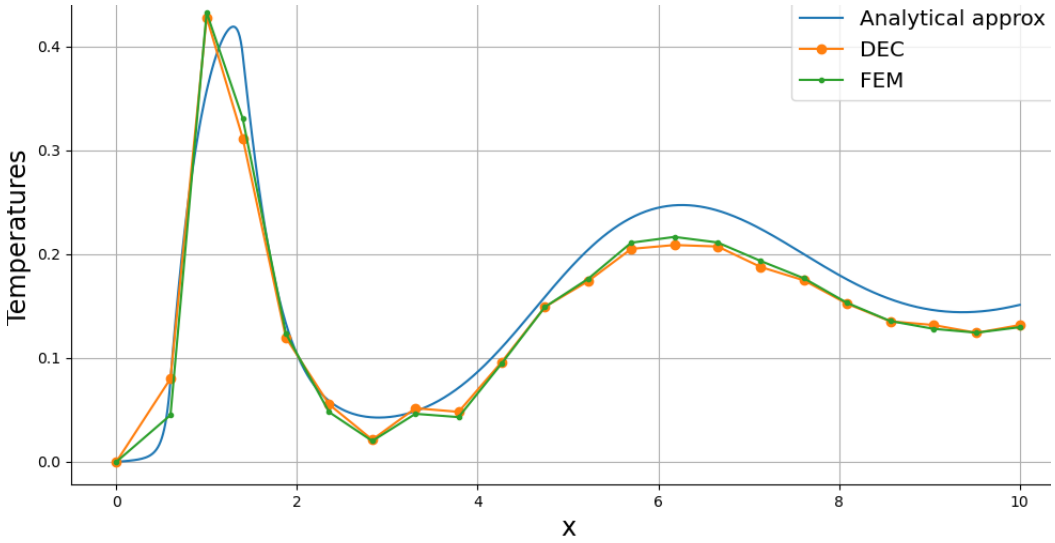

Figure 4.12: Comparision of dynamic solutions on mesh 4.10(b)

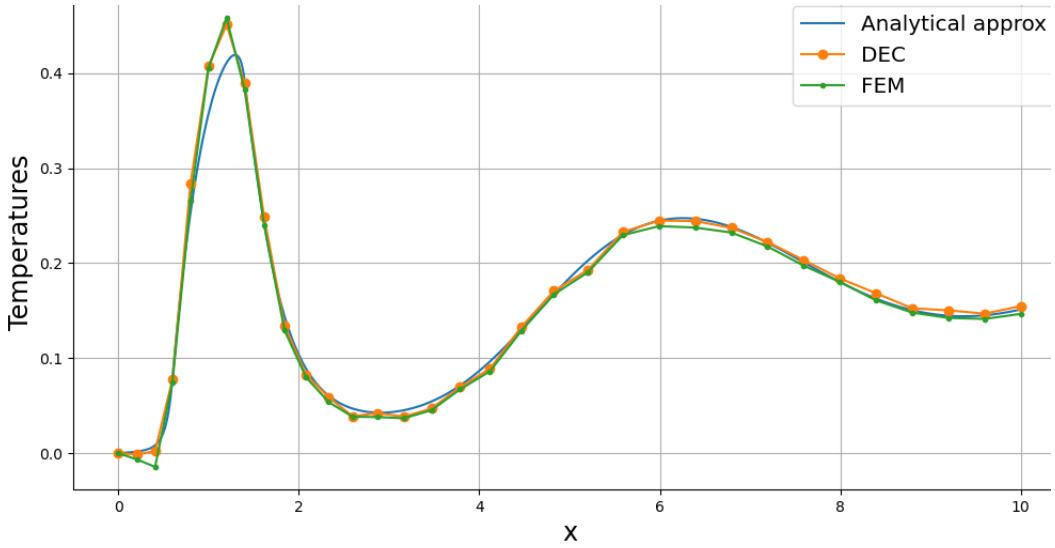

Figure 4.13: Comparision of dynamic solutions on mesh 4.10(c)

We can observe that in the case in figure 4.11 the DEC solution results in a smoother curve than FEM's, while for the other coarse meshes we observe similar behavior on both methods. We can even observe that we get a good approximation using a mesh with just 722 elements for the analytical solution.

On the other hand, we can also observe both methods' performances by comparing cumulative iterations on each time step as shown in figures 4.14, where it is quite notorious that DEC had a better performance on meshes 4.10(a) and 4.10(c) than FEM, while on mesh 4.10(b) both method seems to give similar results. Summarising, we show on table 4.3 the scaled error for both methods

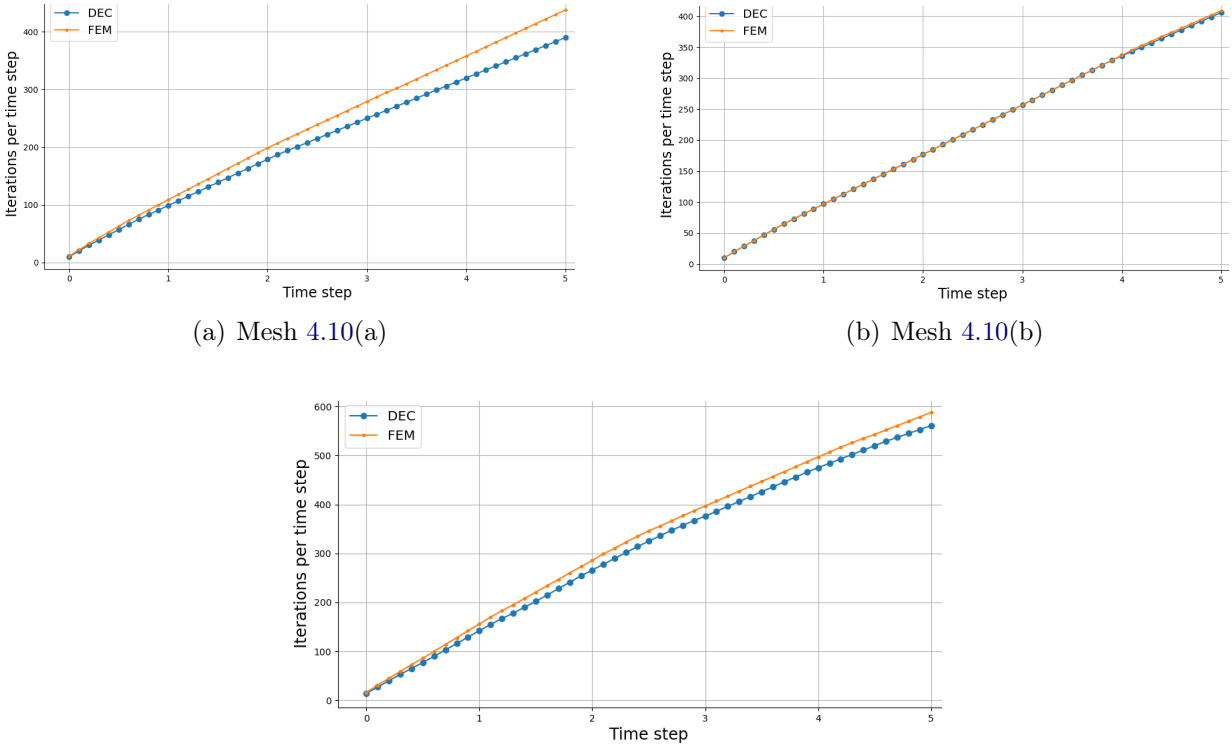

(a) Mesh 4.10(a)

(b) Mesh 4.10(b)

(c) Mesh 4.10(c)

Figure 4.14: Cumulative iterations per mesh

with respect to the analytical approximation along the horizontal symmetry axis and the total cumulative iterations used for DEC and FEM on each mesh. It is easy to see the FEM had a smaller error with respect to DEC's on mesh 4.10(b) while DEC was superior on the other two coarse meshes.

		Scaled error		Total iterations	
Mesh	x points	DEC	FEM	DEC	FEM
Fig. 4.10(a)	15	1.412452×10^{-2}	1.961930×10^{-2}	$10,703$	$11,937$
Fig. 4.10(b)	22	6.643699×10^{-3}	6.311415×10^{-3}	$10,979$	$11,009$
Fig. 4.10(c)	33	2.296155×10^{-3}	2.448873×10^{-3}	$15,788$	$16,722$

Table 4.3: Comparision for dynamic solutions from both methods

4.2 Rotational Velocity Field

For the next numerical example we consider a circular domain with radius $R = 2$ with its characteristics shown in figure 4.15, with the following configuration

- Diffusion coefficient $k = 0.02$
- Vector field $\boldsymbol{u}(x, y) = (y, -x)^T$
- Dynamic coefficient $\nu = 0.1$
- Initial value $\phi_0 = 0$
- Final time $T = 40$
- Interpolation parameter $\theta = 0.6$

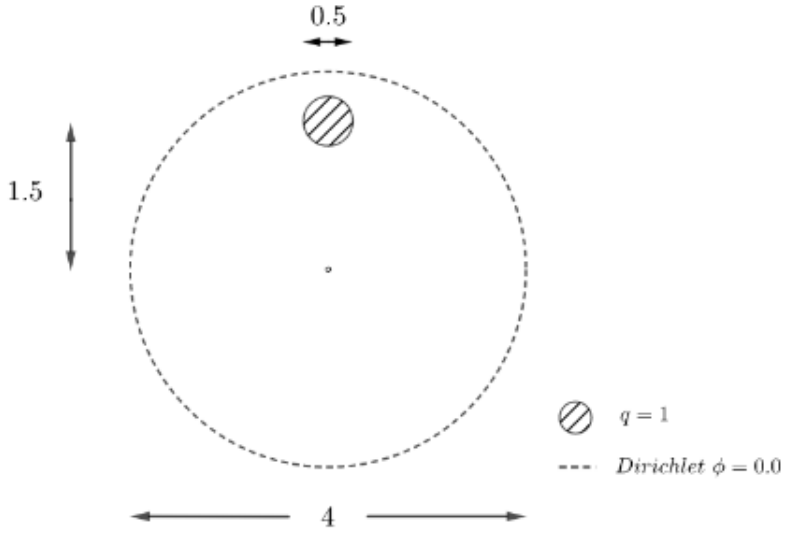

Figure 4.15: Circular domain and its characteristics for numerical experiments

In this case, the mesh used for the static solution consisted of $75,080$ elements so that correction scheme is not needed and we compared its solution with other three fine meshes as shown in figure 4.16 in which we did use dynamic correction scheme with the following configuration

- Parameter for artificial diffusion $\delta = 250$
- Tolerance error $\tau = 10^{-10}$
- Maximum number of iterations $N = 10^4$ on each time step

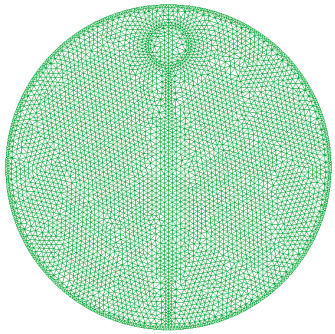

(a) 4,717 nodes and 9,016 elements

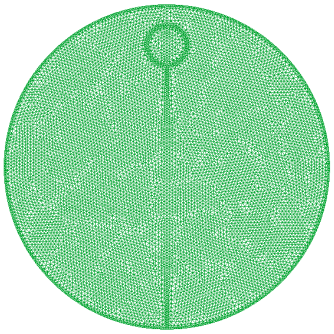

(b) 10,057 nodes and 19,488 elements

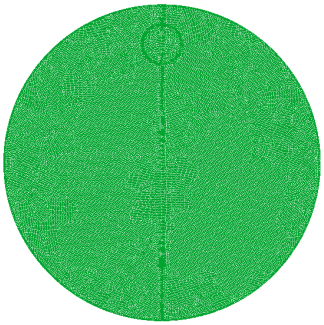

(c) 38,167 nodes and 75,080 elements

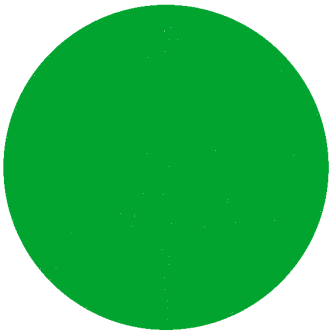

(d) 148,304 nodes and 294,098 elements

Figure 4.16: Fine meshes used for circular geometry

We plot the solutions obtained along the vertical symmetric axis as shown in figure 4.17

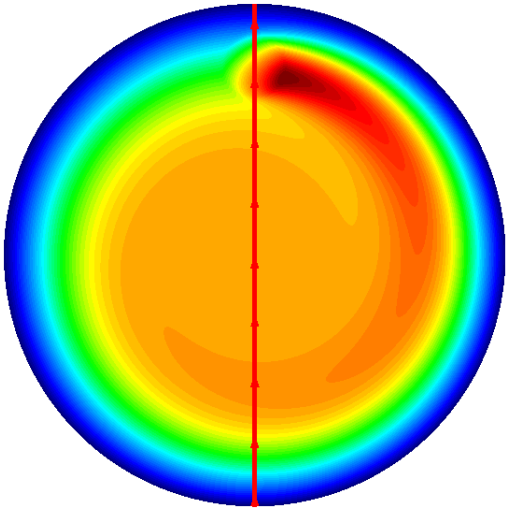

Figure 4.17: Static solution without correction scheme

We show in figure 4.18 the comparision for both methods with static and dynamic correction solutions using fine meshes

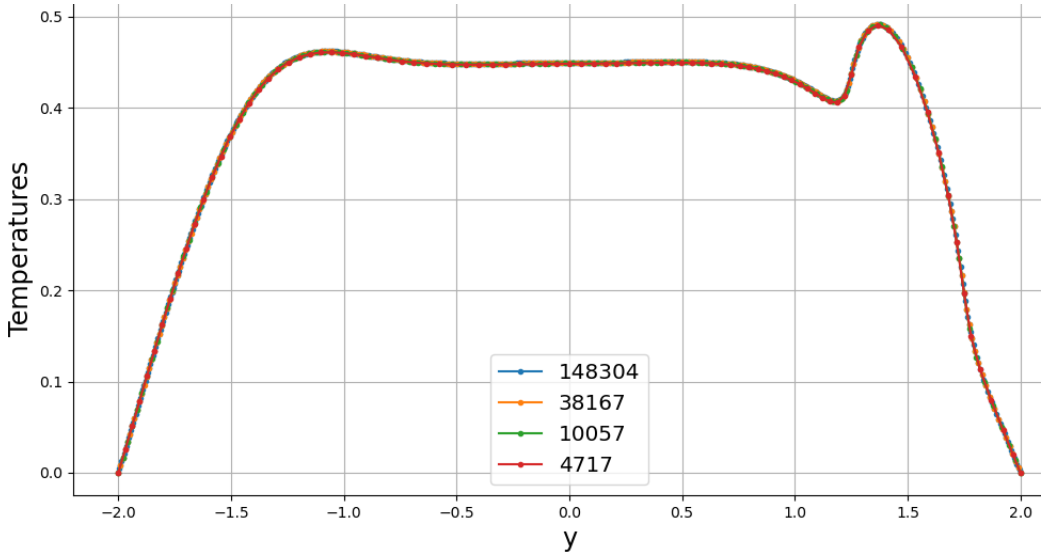

(a) Static and dynamic results using DEC

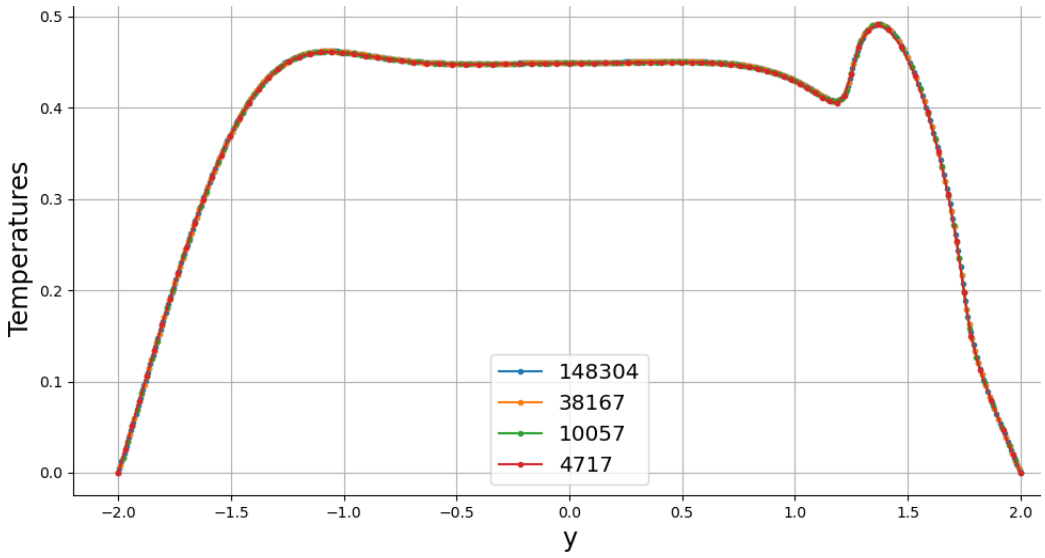

(b) Static and dynamic results using FEM

Figure 4.18: Solutions obtained from DEC and FEM for rotational velocity

Just as in the sinusoidal case, we observe dynamic solutions obtained from both methods match its corresponding static solution, and once again, the dynamic correction scheme is able to approximaye the solution for the original equation by removing artificial diffusion at each time step.

We can see in Figures 4.19, 4.20 and 4.21 that solutions from both methods behave quite similarly on each fine mesh. In table 4.4 we show the comparisions between the solutions of both methods for each mesh.

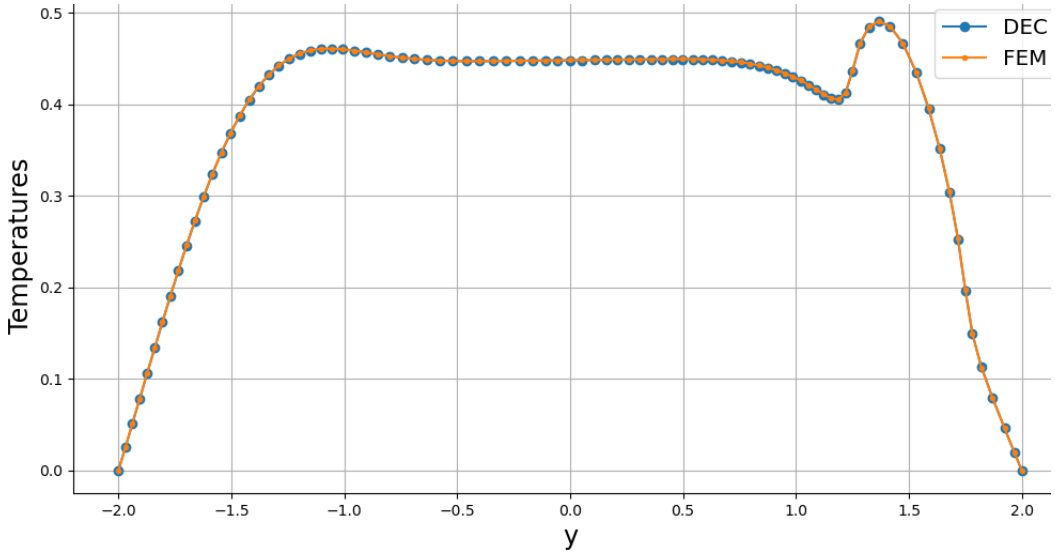

Figure 4.19: Comparision of dynamic solutions from methods on mesh 4.16(a)

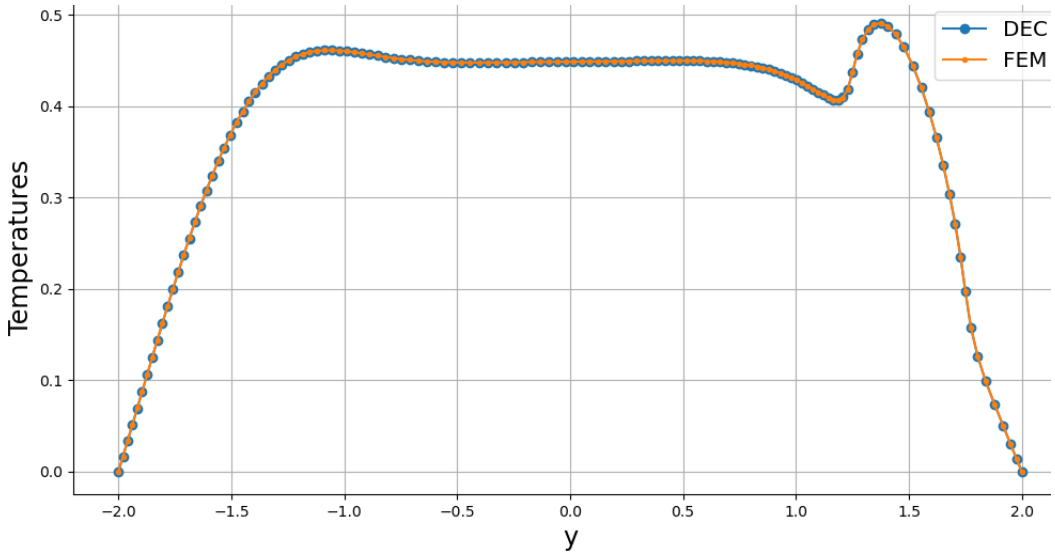

Figure 4.20: Comparision of dynamic solutions from methods on mesh 4.16(b)

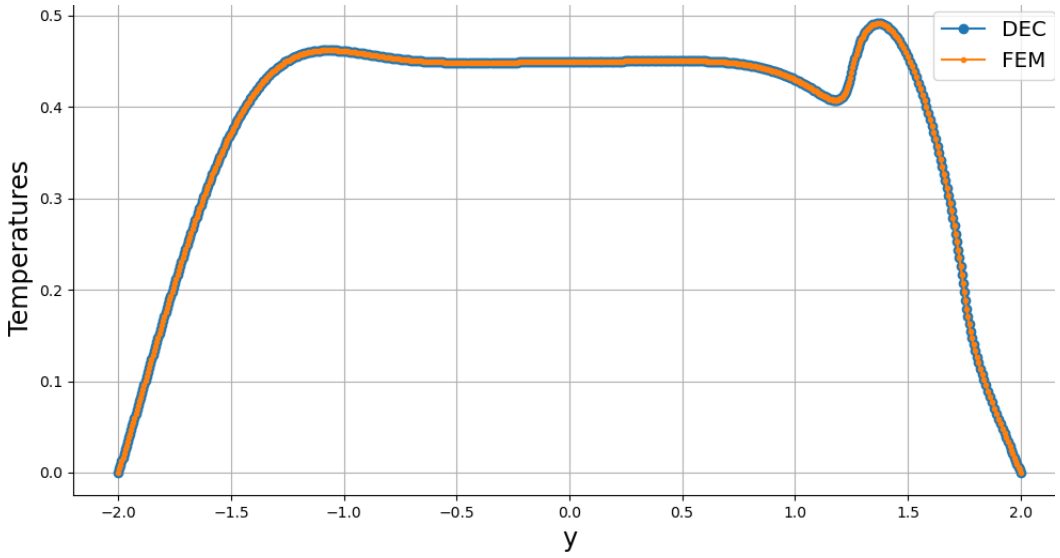

Figure 4.21: Comparision of dynamic solutions from methods on mesh 4.16(b)

We can observe that solutions from both methods on each mesh get quite similar results and we only need a fine mesh like 4.16(b) to get the same solution from DEC and FEM.

Mesh	# Nodes	# Elements	Scaled error	Cosine
Fig. 4.16(a)	4,717	9,016	3.481729×10^{-5}	9.999998×10^{-1}
Fig. 4.16(b)	10,057	19,488	1.052727×10^{-5}	1.000000×10^{0}
Fig. 4.16(d)	148,304	294,098	2.313405×10^{-7}	1.000000×10^{0}

Table 4.4: Comparision for dynamic solutions from both methods

In figure 4.22 we show the number of cumulative iterations per time step for both methods and we observe the same behavior between the methods just as in the sinusoidal case but a completely different behavior as far as fine meshes are concerned. We can see that the finer the mesh the fewer iterations are used for each method.

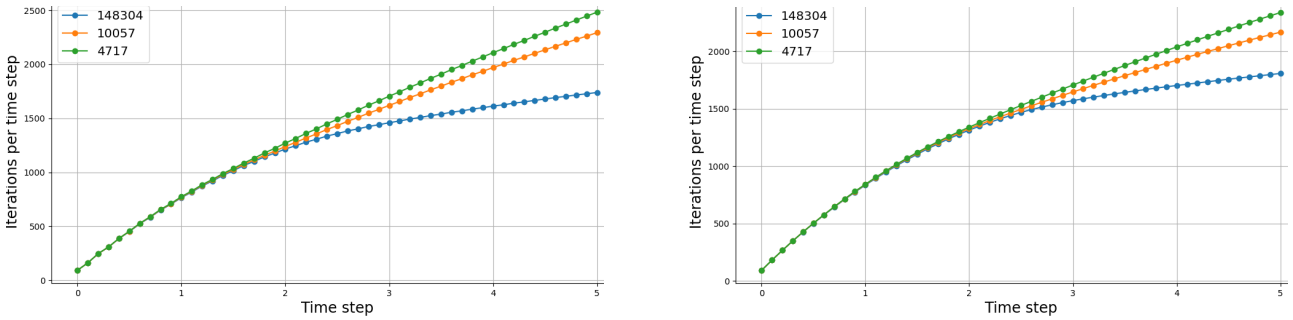

(a) DEC behavior on each fine mesh

(b) FEM behavior on each fine mesh

Figure 4.22: Cumulative iterations per method

Now, we compare on each fine mesh the performance of dynamic correction scheme for both methods as shown on table 4.5 and in figure 4.23 where we can observe DEC used fewer iterations than FEM on each mesh. In fact, the finer the mesh the greater the difference between the iterations used.

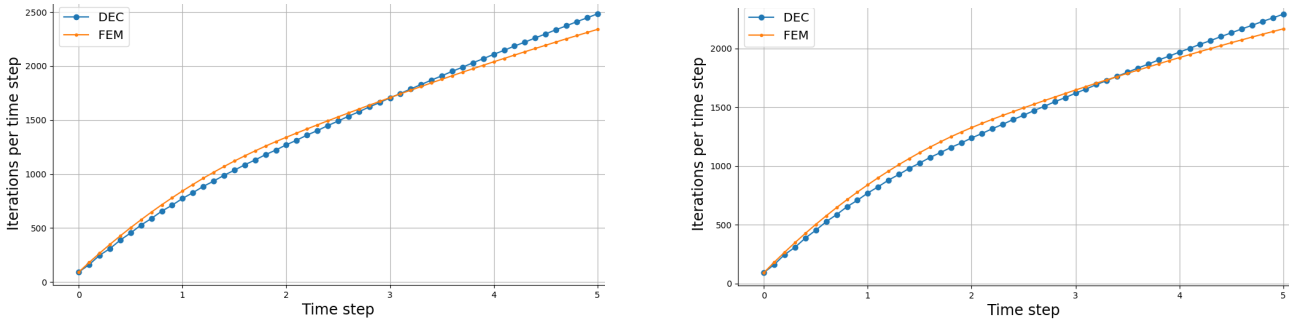

(a) Mesh 4.16(a)

(b) Mesh 4.16(b)

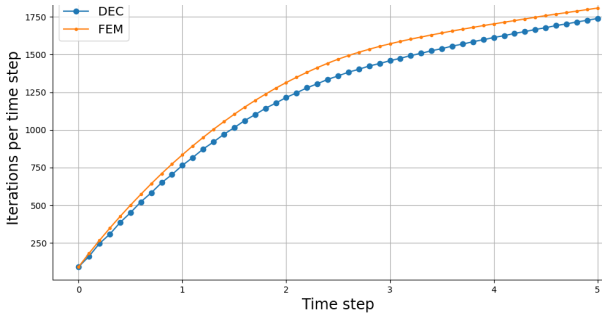

(c) Mesh 4.16(d)

Figure 4.23: Cumulative iterations per mesh

Mesh characteristics			Total iterations	
Mesh	# Nodes	# Elements	DEC	FEM
Fig. 4.16(a)	4,717	9,016	73, 014	73, 165
Fig. 4.16(b)	10,057	19,488	69, 452	70, 352
Fig. 4.16(d)	148,304	294,098	61, 095	65, 350

Table 4.5: Dynamic correction performance of both methods

We now proceed to compare the performance of each method using coarse meshes so that the dynamic correction scheme must to be used (see figure 4.24). We will use the solution for mesh 4.16(d) as the analytical approximation to compare with.

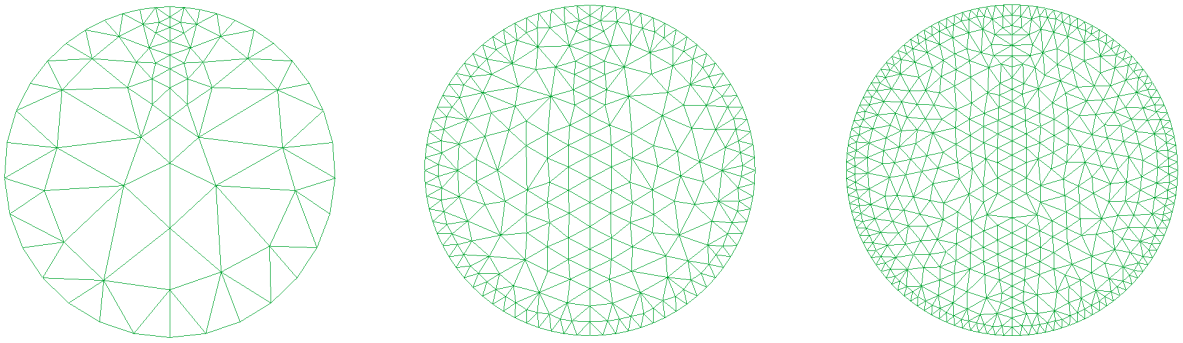

(a) 4,717 nodes and 9,016 elements

(b) 10,057 nodes and 19,488 elements

(c) 38,167 nodes and 75,080 elements

Figure 4.24: Coarse meshes used for circular geometry

Figures 4.25, 4.26 and 4.27 shows the results obtained on coarse meshes from both methods.

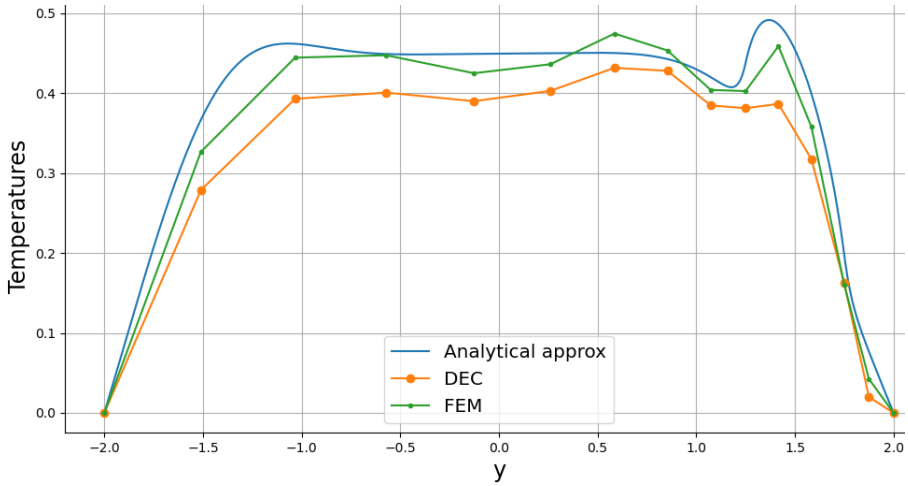

Figure 4.25: Comparision of dynamic solutions on mesh 4.24(a)

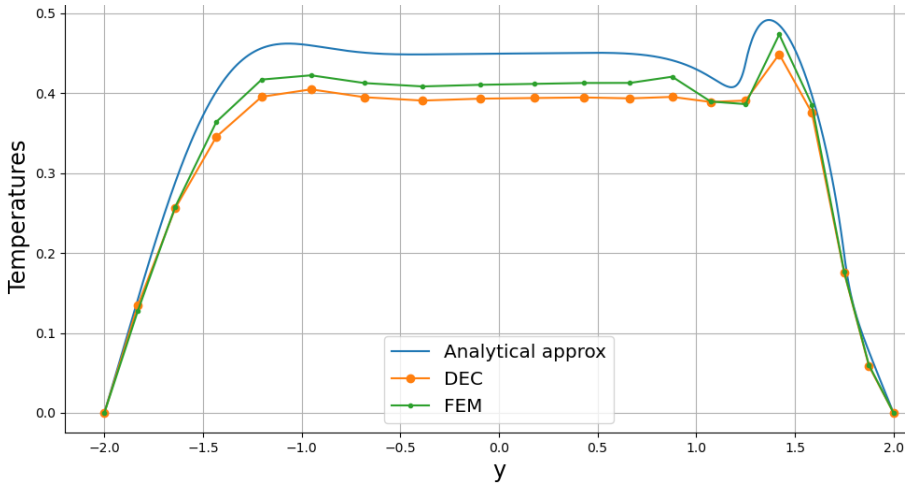

Figure 4.26: Comparision of dynamic solutions on mesh 4.24(b)

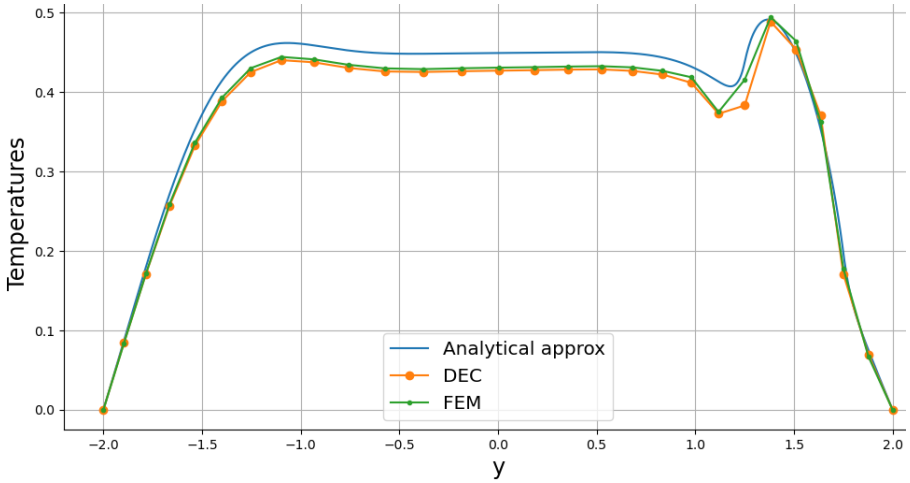

Figure 4.27: Comparision of dynamic solutions on mesh 4.24(c)

In this case, we observe the opposite behavior to the sinusoidal velocity field, FEM seems to have better results for coarse meshes than DEC. This can be due to the shape of the triangles for each mesh, because DEC captures the information of the velocity field $\boldsymbol{u}$ on each vertex while FEM only uses the value of $\boldsymbol{u}$ on the triangle's barycenter. As a matter of fact, we can observe that the triangles in the coarse meshes of the rectangular domain are not as distorted as the triangles of coarse meshes of the circular domain. This may explain why there are better DEC results, in comparision with FEM, for the previous case than in this one.

We can also observe both methods' performances by comparing cumulative iterations at each time step as shown in figure 4.28.

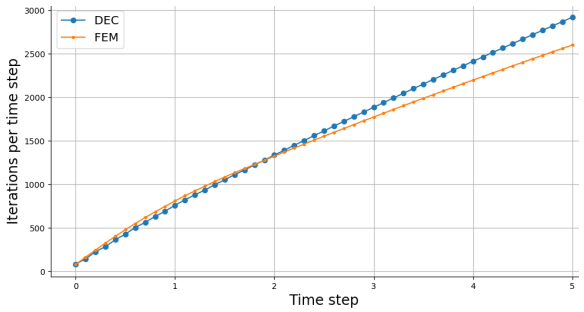

(a) Mesh 4.24(a)

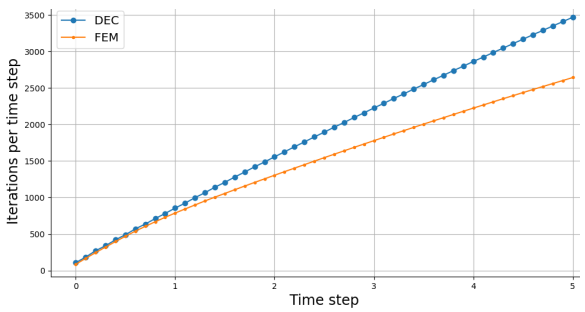

(b) Mesh 4.24(b)

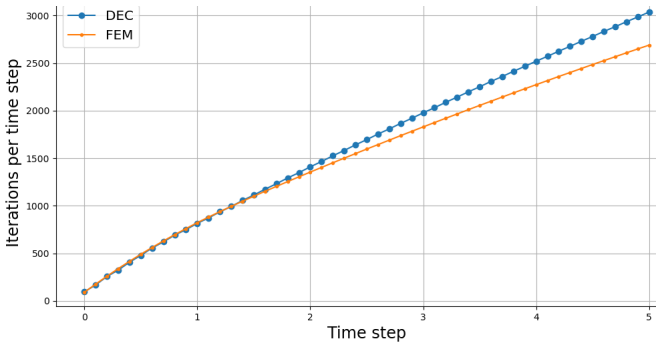

(c) Mesh 4.24(c)

Figure 4.28: Cumulative iterations per mesh

Where we can see, once again, FEM used fewer iterations than DEC on all coarse meshes, which reinforces the previous explanation.

Summarising, we show in table 4.6 the scaled error for both methods with respect to the analytical approximation along the vertical symmetry axis and total cumulative iterations used for DEC and FEM on each mesh. As previously mentioned, FEM's performance was better than DEC's both in solution obtained and total number of iterations used during dynamic scheme correction.

		Scaled error		Total iterations	
Mesh	y points	DEC	FEM	DEC	FEM
Fig. 4.24(a)	15	1.439571×10^{-2}	0.663578×10^{-2}	80,639	76,233
Fig. 4.24(b)	20	9.735095×10^{-3}	6.953187×10^{-3}	94,860	76,324
Fig. 4.24(c)	28	4.218274×10^{-3}	3.237909×10^{-3}	84,639	78,446

Table 4.6: Comparision for dynamic solutions from both methods

4.3 Rotational Velocity with disturbances

For the final numerical example we consider an square domain with side $L = 4$ and its characteristics can be seen in figure 4.29.

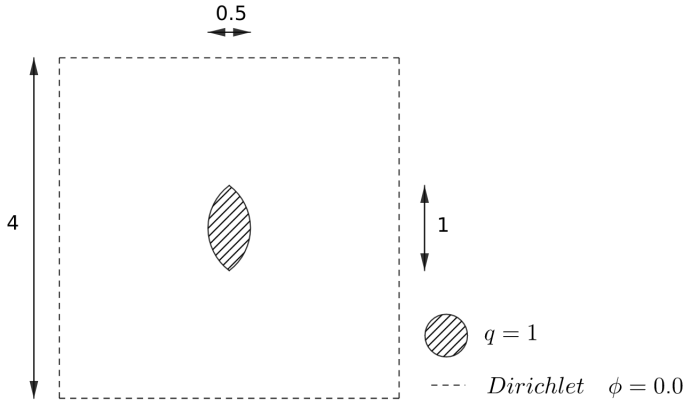

Figure 4.29: Square domain and its characteristics for numerical experiments

In this example our main goal is to show how different the solutions are when we consider a significant field divergence on transport equation, here we consider the following configuration

- Diffusion coefficient $k = 0.02$
- Vector field $\boldsymbol{u} = (-y, x)^T + \epsilon(x, y)^T$, $\epsilon \in \{0.0, 0.5, 2.0\}$
- Dynamic coefficient $\nu = 0.05$
- Initial value $\phi_0 = 0$
- Final time $T = 21$
- Interpolation parameter $\theta = 0.6$

We will use one fine, regular and coarse meshes, as shown in figure 4.30, for different values of ϵ and the dynamic correction scheme will only be used for regular and coarse meshes. Since the geometry for this example allows us to work with triangles which are not very obtuse, DEC is the best option for solving it, therefore we only use DEC.

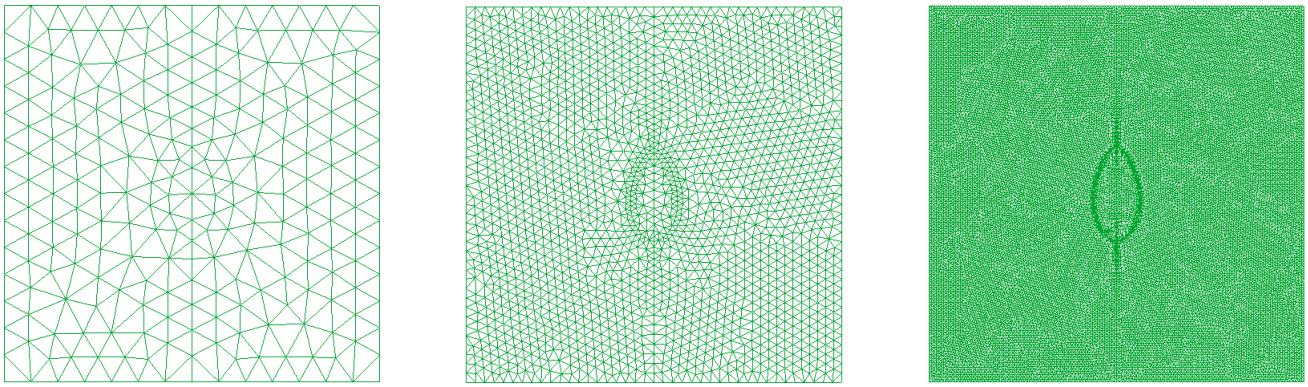

(a) 242 nodes and 426 elements

(b) 1,941 nodes and 3,720 elements

(c) 20,941 nodes and 41,344 elements

Figure 4.30: Coarse, regular and fine meshes used for square geometry, respectively

The static solutions obtained on the finer mesh for different ϵ values are shown in figure 4.31.

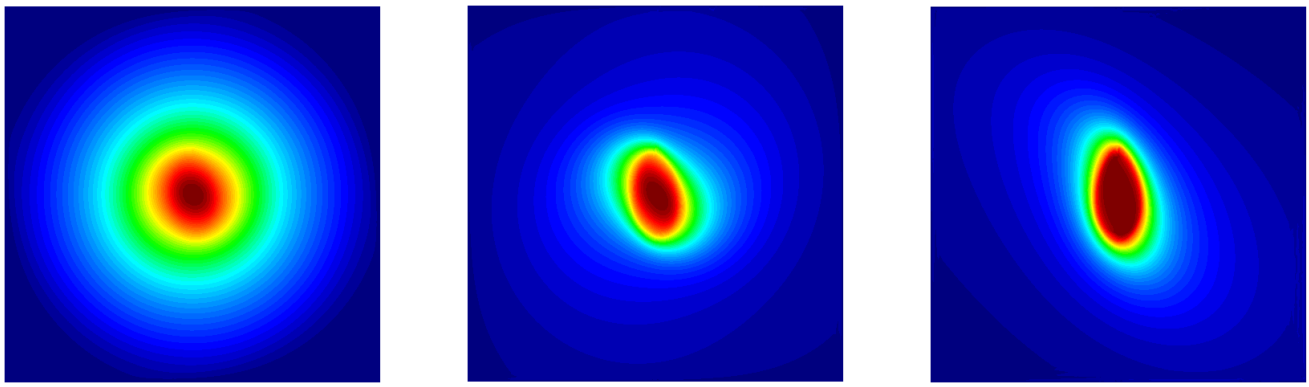

(a) $\epsilon = 0.0$

(b) $\epsilon = 0.5$

(c) $\epsilon = 2.0$

Figure 4.31: Solutions for different ϵ values on mesh 4.30(c)

It is quite notorious the effect of a strong field divergence perturbation, the temperatures distribution changes all over the domain, we notice the larger ϵ gets, the more the distribution loses radial symmetry. In order to compare how the distribution changes, we plot the solutions obtained along the horizontal and vertical symmetry axes for the coarse and regular meshes using the following configuration for the dynamic correction scheme

- Parameter for artificial diffusion $\delta = 250$
- Tolerance error $\tau = 10^{-10}$
- Maximum number of iterations $N = 10^4$ on each time step

First, we show in figures 4.32 and 4.33 how the distribution of the solution changes over the domain for ϵ values on horizontal and vertical axes, respectively, for the finest mesh.

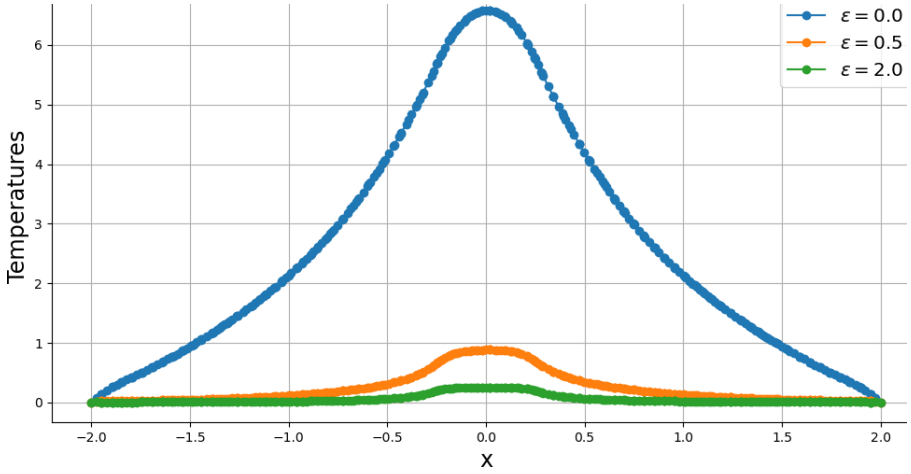

Figure 4.32: Temperature variation along horizontal symmetric axis

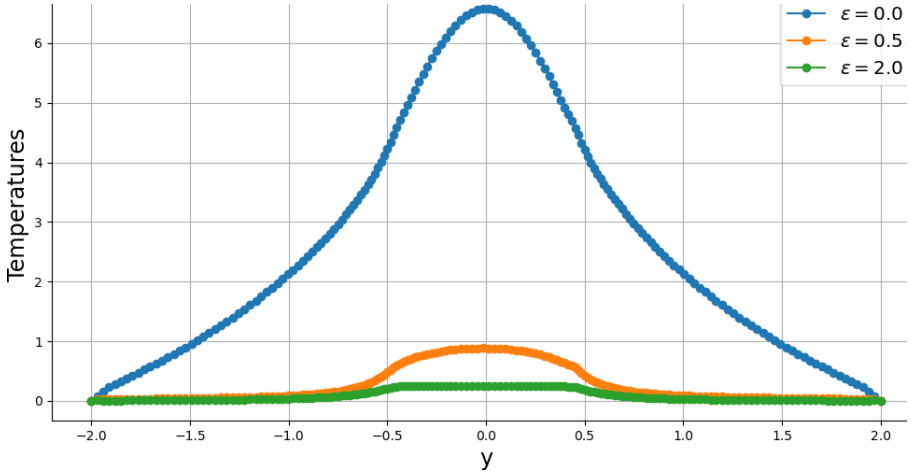

Figure 4.33: Temperature variation along vertical symmetric axis

Clearly, the larger ϵ the more the temperature distribution decreases along both horizontal and vertical axes. Now we proceed to show the solutions obtained on each mesh for both axis with $\epsilon = 0.0, 0.5, 2.0$ in figures 4.34, 4.35 and 4.36, respectively.

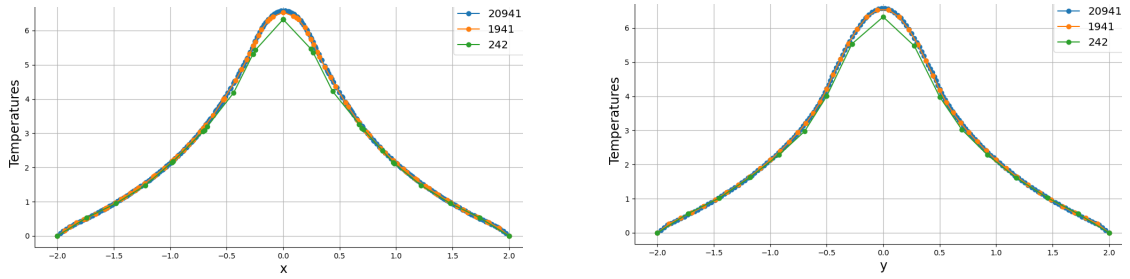

Figure 4.34: Solutions for $\epsilon = 0.0$ on each mesh for both axis

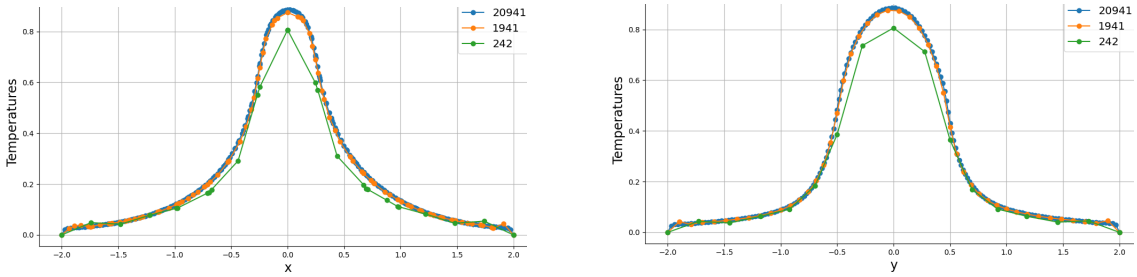

Figure 4.35: Solutions for $\epsilon = 0.5$ on each mesh for both axis

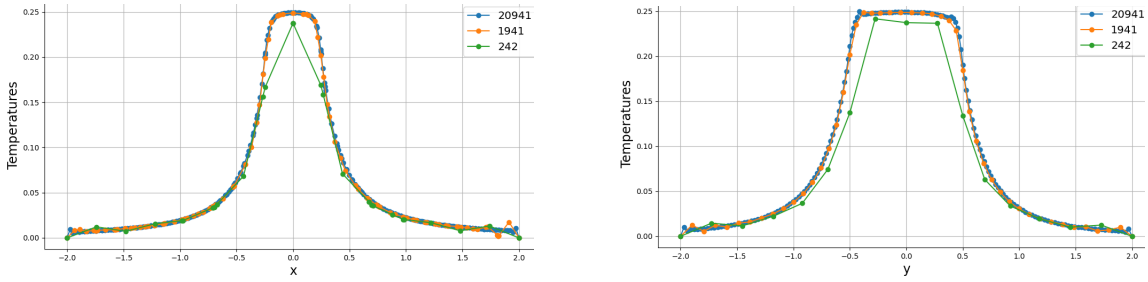

Figure 4.36: Solutions for $\epsilon = 2.0$ on each mesh for both axis

We can observe that symmetry is indeed lost, the temperature distribution on horizontal axis is thinner than on vertical axis regardless of the mesh.

It is interesting to ask, what happens with the performance of the dynamic correction scheme when the field divergence increases? This can be answered by looking at Figures 4.37 and 4.38, where we can observe that it is way faster to remove artificial diffusion when there is a non-zero divergence, this may be due to the elemental matrix associated to field divergence term $(\boldsymbol{\nabla} \cdot \boldsymbol{u})\phi$, since it is a diagonal matrix, it does not destabilize the transport equation unlike the directional derivative term $\boldsymbol{u} \cdot \boldsymbol{\nabla}\phi$.

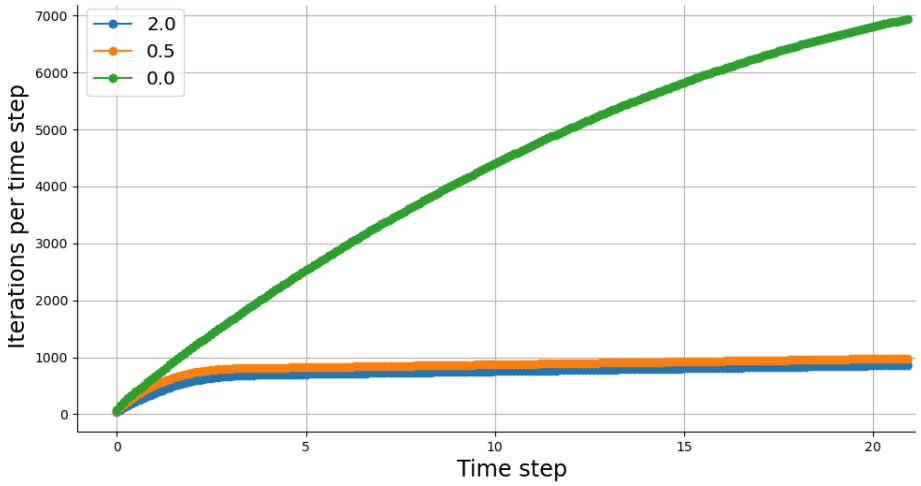

Figure 4.37: Cumulative iterations for ϵ values on mesh 4.30(a)

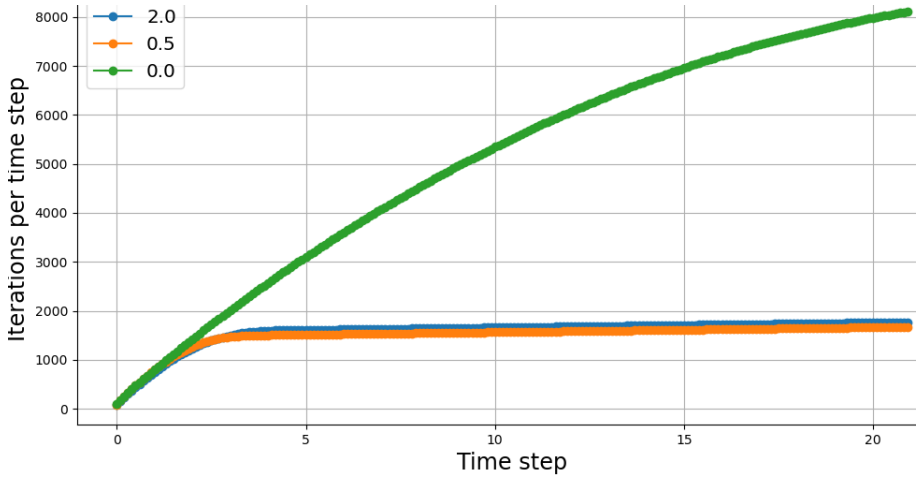

Figure 4.38: Cumulative iterations for ϵ values on mesh 4.30(b)

Summarising, we show the results of the comparision for the solutions obtained with the coarse and regular meshes with the fine mesh for each ϵ value in table 4.7.

		Scaled error		
$\nabla \cdot \boldsymbol{u} = 2\epsilon$	Mesh	x axis	y axis	Total iterations
$\epsilon = 0.0$	Fig. 4.30(a)	3.127980×10^{-2}	3.455932×10^{-2}	$885,224$
	Fig. 4.30(b)	0.185643×10^{-2}	0.170706×10^{-2}	$1'061,080$
$\epsilon = 0.5$	Fig. 4.30(a)	1.014965×10^{-2}	1.020167×10^{-2}	$177,608$
	Fig. 4.30(b)	0.079939×10^{-2}	0.095330×10^{-2}	$313,365$
$\epsilon = 2.0$	Fig. 4.30(a)	2.519354×10^{-3}	5.869518×10^{-3}	$152,163$
	Fig. 4.30(b)	0.277767×10^{-3}	0.421625×10^{-3}	$329,690$

Table 4.7: Comparision for solutions for ϵ values on coarse and regular meshes

Chapter 5

Conclusions and Future Work

Discrete exterior calculus is a numerical method for partial differential equations that that was introduced almost 20 years ago. Many discretization proposals have been made for differential terms that appear on a wide variety of partial differential equations. However, the transport equation has two important situations as far as DEC is concerned

1-. Full convective term discretization $\boldsymbol{\nabla} \cdot (\boldsymbol{u}\phi) = (\boldsymbol{\nabla} \cdot \boldsymbol{u})\phi + \boldsymbol{u} \cdot \boldsymbol{\nabla}\phi$

2-. Numerical instability for dominant convection

In this thesis, we worked and solved both situations. The key idea to solve the first one is to understand that we build discrete operators (matrices) conrresponding to differential operators acting on unknown quantities, such as ϕ and $\boldsymbol{u} \cdot \boldsymbol{\nabla}\phi$. However, we must proceed differently with the term $(\boldsymbol{\nabla} \cdot \boldsymbol{u})\phi$, since the differential operation, divergence, acts on the known quantity $\boldsymbol{u}$. Thus, we treat the scalar term $\boldsymbol{\nabla} \cdot \boldsymbol{u}$ as a $0-$form $f = \boldsymbol{\nabla} \cdot \boldsymbol{u}$. This is also applied for finite element method (FEM) and we showed there is consistency for both methods.

For the second situation, we must deal with dominant convection by using artificial diffusion on the transport equation which is a common way to stabilize this equation. Nevertheless, since we are modifying the equation, the stabilized solution obtained will not be the solution for the original phenomena.

We proposed an iterative algorithm, correction scheme, to remove artificial diffusion once the

system of equations has been stabilized in order to solve correctly the original equation. We showed this scheme not only works for both DEC and FEM, but also it is faster when working on meshes whose elements (triangles) and not very obtuse, and for vector fields with non-zero divergence.

We also showed DEC is a numerical method able to compete with FEM because it obtains more information over the elemental formulation for all the terms (vertices and edges) while FEM simplifies it on convective and dynamic terms. This can result in an advantage or disadvantage for DEC and it will depend on how distorted the triangular elements are.
As a continuation of this work, it is planned to work with non-autonomous vector fields $\boldsymbol{u} = \boldsymbol{u}(t, x, y)$ in the transport equation.

Bibliography

[1] Anil Nirmal Hirani. *Discrete exterior calculus*. California Institute of Technology, 2003.

[2] Anil N Hirani, Kalyana B Nakshatrala, and Jehanzeb H Chaudhry. Numerical method for darcy flow derived using discrete exterior calculus. *International Journal for Computational Methods in Engineering Science and Mechanics*, 16(3):151–169, 2008.

[3] Jukka Räbinä. On a numerical solution of the maxwell equations by discrete exterior calculus. *Jyväskylä studies in computing*, (200), 2014.

[4] Mamdouh S Mohamed, Anil N Hirani, and Ravi Samtaney. Discrete exterior calculus discretization of incompressible navier–stokes equations over surface simplicial meshes. *Journal of Computational Physics*, 312:175–191, 2016.

[5] Marco Antonio Noguez Morales. *Discretización de la ecuación convección-difusión con cálculo exterior discreto*. Centro de Investigación en Matemáticas, 2019.

[6] Michael Griebel, Christian Rieger, and Alexander Schier. Upwind schemes for scalar advection-dominated problems in the discrete exterior calculus. In *Transport Processes at Fluidic Interfaces*, pages 145–175. Springer, 2017.

[7] Humberto Esqueda Oliva. *Cálculo exterior discreto en la solución de EDPs: formulación local para problemas térmicos anisótropos*. Centro de Investigación en Matemáticas, 2021.